SECURITY CLASSIFICATION OF THIS PAGE *(When Data Entered)*

REPORT DOCUMENTATION PAGE	READ INSTRUCTIONS BEFORE COMPLETING FORM

1. REPORT NUMBER NAVENVPREDRSCHFAC Contractor Report CR 84-05	2. GOVT ACCESSION NO.	3. RECIPIENT'S CATALOG NUMBER

4. TITLE *(and Subtitle)* Simple Mesoscale Models for Operational Use in Regions of Topographic and Thermal Forcing: Development and Evaluation	5. TYPE OF REPORT & PERIOD COVERED Final
	6. PERFORMING ORG. REPORT NUMBER

7. AUTHOR(s) Dr. Clifford F. Mass	8. CONTRACT OR GRANT NUMBER(s) N00014-82-K-0674

9. PERFORMING ORGANIZATION NAME AND ADDRESS Department of Atmospheric Sciences University of Washington Seattle, WA 98195	10. PROGRAM ELEMENT, PROJECT, TASK AREA & WORK UNIT NUMBERS PE 63207N PN 7W0513 TA CC00 NEPRF WU 6.3-8

11. CONTROLLING OFFICE NAME AND ADDRESS Naval Air Systems Command Department of the Navy Washington, DC 20361	12. REPORT DATE July 1984
	13. NUMBER OF PAGES 86

14. MONITORING AGENCY NAME & ADDRESS *(If different from Controlling Office)* Naval Environmental Prediction Research Facility Monterey, CA 93943	15. SECURITY CLASS. *(of this report)* UNCLASSIFIED
	15a. DECLASSIFICATION/DOWNGRADING SCHEDULE

16. DISTRIBUTION STATEMENT *(of this Report)*

Approved for public release; distribution is unlimited.

17. DISTRIBUTION STATEMENT *(of the abstract entered in Block 20, if different from Report)*

18. SUPPLEMENTARY NOTES

19. KEY WORDS *(Continue on reverse side if necessary and identify by block number)*

Mesoscale modeling
Topographic forcing
Modeling
Numerical modeling
Limited area modeling
Complex terrain

20. ABSTRACT *(Continue on reverse side if necessary and identify by block number)*

A one-level numerical (Mass-Dempsey) model suitable for diagnosing mesoscale flow in regions of complex terrain and land/water interface is described. This model requires only modest computer resources and needs little data for initialization. Two other one-level models also are described and run with the Mass-Dempsey model for cases of the Pacific Northwest, San Francisco Bay Area, and Subic Bay, PI. Results suggest that the Mass-Dempsey model produces fairly

((continued on reverse))

DD FORM 1473 1 JAN 73 · EDITION OF 1 NOV 65 IS OBSOLETE
S/N 0102-014-6601

Block 20, Abstract, continued.

good results and appears to be superior to the other models. It is also found, however, that the model requires too much computer resources for operational use on small computers.

```
AB  (27)  A one-level numerical (Mass-Dempsey) model suitable for
          diagnosing mesoscale flow in regions of complex terrain
          and land/water interface is described. This model
          requires only modest computer resources and needs
          little data for initialization. Two other one-level
          models also are described and run with the Mass-Dempsey
          model for cases of the Pacific Northwest, San Francisco
          Bay Area, and Subic Bay, Pl. Results suggest that the
          Mass-Dempsey model produces fairly good results and
          appears to be superior to the other models. It is also
          found, however, that the model requires too much
          computer resources for operational use on small
          computers.
```

NAVENVPREDRSCHFAC CR 84-05

SIMPLE MESOSCALE MODELS FOR OPERATIONAL USE IN REGIONS OF TOPOGRAPHIC AND THERMAL FORCING: DEVELOPMENT AND EVALUATION

Prepared By:

Dr. Clifford F. Mass
Department of Atmospheric Sciences
University of Washington
Seattle, WA 98195

JULY 1984

Prepared For:

NAVAL ENVIRONMENTAL PREDICTION RESEARCH FACILITY,
MONTEREY, CALIFORNIA 93943

CONTENTS

1. Introduction

During the past decade the performance of synoptic scale numerical models has improved substantially; however, even if these models could forecast large scale features perfectly, the problem of translating this information into mesoscale and local weather remains. Such translation is particularly difficult in regions of complex terrain[1] or land/water interface where topographic deflection and channeling, thermally driven land/sea breezes and mountain/valley winds, and differential friction all contribute to the weather in the lower troposphere. Of course, one might avoid the translation completely by running current operational models with sufficient spacial and temporal resolution to resolve these mesoscale circulations; unfortunately, this approach would require enormous and currently unavailable computer resources.

One solution to this synoptic to mesoscale translation problem is to develop diagnostic, limited-area, mesoscale numerical models capable of producing mesoscale flows consistent with larger scale fields. Such diagnostic models could be applied to the output of prognostic, synoptic scale models or to current or historic synoptic observations to provide meteorological fields of greater resolution and detail. One candidate might be the class of three dimensional primitive equation

---

[1] In subsequent references in this report, "complex terrain" will indicate both topographic relief and land/water contrast.

models (e.g., Anthes and Warner, 1978; Pielke, 1974; Nickerson and Magaziner, 1976) that appear to model flow in complex terrain satisfactorily if given sufficient data for initialization and boundary specification. Unfortunately, such data are rarely available in regions of complex terrain. In addition, these models require enormous computer resources, far in excess of that available at local forecast offices and even at most numerical forecast centers. The obvious question is then: can simpler models requiring more modest computer resources be developed? Furthermore, can these models be constructed so that they require little initial data? To answer these questions a more fundamental question must also be addressed: What are the essential physics necessary to realistically model flow in complex terrain?

Attempts to develop simplified models for diagnosing and forecasting mesoscale meteorological phenomena in regions of complex terrain can generally be divided into three types: mass conservation models, one-layer primitive equation models that assume a well-mixed boundary layer, and one-level sigma coordinate models that use the primitive equation set without the continuity equation.

The mass conservation models (e.g., Anderson, 1971; Fosberg et. al., 1976; Dickerson, 1978; Sherman, 1978) integrate the mass continuity equation through a specified layer of topographic influence. These models neglect non-linear advection, the coriolis force and adiabatic warming and cooling, and cannot realistially simulate thermal circulations. Such limited physics suggests that these models are most appropriate for smaller domains with stable flow, moderate topographic relief and weak or nonexistent diurnal circulations. The mass

2

conservation models do have the advantage of requiring only a large scale wind field and the depth of the layer of influence as input and need only modest computer resources.

The second group of simplified mesoscale models are based on the mixed layer model of Lavoie (1972). These models (e.g. Lavoie, 1972, 1974; Overland et. al., 1979; Keyser and Anthes, 1977) divide the lower atmosphere into four layers: a surface layer of constant stress, a well-mixed boundary layer, an inversion layer and the free atmosphere above. Mixed layer height, wind and potential temperature are integrated in time using vertically integrated forms of the primitive equations that include nonlinear advection, coriolis acceleration, boundary layer entrainment and friction. Requiring only large scale geostrophic winds, mixed layer heights along inflow boundaries and the temperature change across a capping inversion for their initialization, these models can be integrated to a steady state or used for short-term forecasts. Their output appears to duplicate some features of the boundary layer flow in the regions of complex terrain in which they were tested. However, their limitation to well-mixed situations, difficulty in handling large topographic relief, great sensitivity to the boundary values of the mixed layer heights, and other difficulties, leaves substantial room for further development. Furthermore, their specification of mass conservation causes boundary layer heights to progressively fall if net outflow occurs on the boundaries.

The third type of simplified model is a one-level version of the primitive equations (without the continuity equation) in sigma coordinates. This model type was first developed by Danard (1977), whose model parameterizes diabatic effects and boundary layer friction

3

but does not demand mass conservation. The only required inputs are the surface and 850 mb geostrophic winds, the vertical stability of the lower troposphere, and specified air temperatures over land and water. The model is integrated to a steady state and requires only modest computer resources. Danard's results suggest some ability to simulate topographic deflection and channeling even though the model runs were made on an excessively limited domain. A version of the Danard model with better numerics, boundary conditions and diabatic heating parameterization was run on a larger domain in Mass (1981b). Although there were some discrepancies between simulated and observed wind fields, the model appeared to duplicate many aspects of the topographically forced mesoscale flow of the test region.

This report describes the results of running model simulations using three simple models:

(1) A one-level sigma coordinate model that refines and departs from the Danard (1977) and Mass (1981) models. The following section describes this model.

(2) A one-level mixed layer model based on Lavoie (1972), i.e. the model described in Overland et al. (1979).

(3) A multi-level mass continuity model described in Sherman (1978).

The goal of this work is to evaluate the potential of the above three models for diagnosing low-level flow in regions of complex terrain and land/water interface.

2. Description of the one-level sigma coordinate Mass-Dempsey model

a. Basic equations

This one-level model integrates in time the dependent variables, T_s and $\vec{V}_s$, at the surface (or $\sigma = 1$) level (see Fig. 1). The model assumes hydrostatic balance, a restriction valid for all but the smallest scales (less than a few km) or for strong flow rapidly accelerated by highly curved slopes. The model's horizontal momentum equation in sigma coordinates at the surface is:

$$\frac{\partial \vec{V}_s}{\partial t} = -\vec{V}_s \cdot \nabla_\sigma \vec{V}_s - f\vec{k}x\vec{V}_s - (g \vec{\nabla}_\sigma z_s + RT_s \vec{\nabla}_\sigma \ln p_s) - \vec{F} + K_m \nabla_\sigma^2 \vec{V}_s \tag{1}$$

where $\vec{V}_s$, T_s, p_s and z_s are the wind vector, temperature (K), pressure and height at the surface; f is the coriolis parameter, g is the gravitational acceleration, R is the ideal gas constant, $\vec{F}$ is the frictional force and K_m is the horizontal momentum diffusion coefficient. Equation (1) indicates that the wind vector at a point on the surface can be altered by advection, coriolis acceleration, the pressure gradient force, frictional drag and by horizontal diffusion. This diffusion parameterizes subgrid scale horizontal mixing that cannot be resolved by the model and also helps to maintain computational stability. The friction and horizontal diffusion parameterizations are described in Appendixes I and II.

The model's thermodynamic energy equation can be derived by starting with the first law of thermodynamics
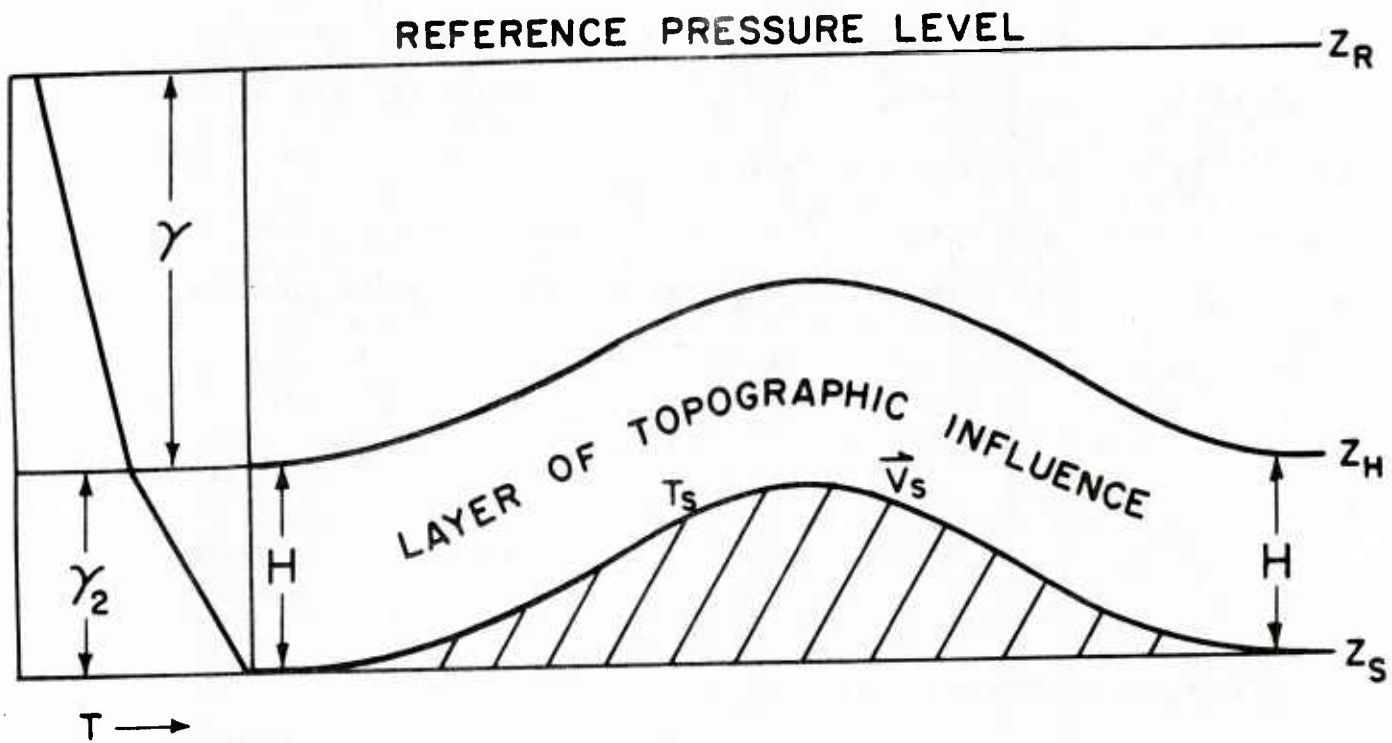
$$c_p \frac{dT}{dt} - \alpha\omega = Q \tag{2}$$

Figure 1.   Vertical structure of the model.

where α is specific volume ($\frac{RT}{p}$), c_p is the heat capacity of dry air, Q is the diabatic heating rate and $\omega = dp/dt$. In sigma coordinates ω can be expressed as

$$\omega = \frac{dp}{dt} = \frac{d}{dt}(p_s\sigma) = p_s\dot\sigma + \sigma\dot p_s \tag{3}$$

Substituting this expression into (2), expanding the total derivative dT/dt, and applying the resulting equation at the surface ($\sigma = 1$, $\dot\sigma = 0$) gives

$$\frac{\partial T_s}{\partial t} + \vec V_s \cdot \vec\nabla_\sigma T_s - \frac{RT_s}{c_p}\left(\frac{\partial \ln p_s}{\partial t} + \vec V_s \cdot \vec\nabla_\sigma \ln p_s\right)$$
$$= \frac{Q}{c_p} + K_t\nabla^2 \sigma T_s \tag{4}$$

where a horizontal diffusion term has been included.

The final unknown, the surface pressure p_s, can be found by integrating the hydrostatic equation from the surface to a level at which the flow is assumed to be unaffected by topographic forcing. As a first step we assumed that the depth of topographic influence above the surface, H, is a constant and can be approximated by 2 km. Admittedly, this assumption is open to question; however, after examining several empirical studies (e.g., Reed, 1981; Marwitz, 1983), this depth appeared to be a reasonable first guess for a wide variety of conditions. Another model requirement is that there exists some constant pressure reference level that is unaffected by the underlying topography. In our model runs for the Pacific Northwest the 850 mb level has been used; higher levels would be appropriate in areas of particularly high terrain. The reference level is used as the upper level from which the hydrostatic equation is integrated down to the

7

surface. Combining the hydrostatic equation and perfect gas law and integrating from the surface to the reference pressure level (p_R) gives

$$\ln p_S = \ln p_R + \left(\frac{g}{R}\right) \int_{z_S}^{z_R} \frac{1}{T(z)} \, dz \tag{5}$$

where z_R is the height of the reference pressure level. If we assume a linear lapse rate, γ, between the reference level (z_R) and the top of the topographic influence layer ($z_S + H$) so that

$$T_{z_S + H} = T_{z_R} + \gamma(z_R - z_S - H) \tag{6}$$

then (5) can be expressed

$$\ln p_S = \ln p_R + \frac{g}{R} \int_{z_S}^{z_S + H} \frac{1}{T(z)} \, dz + \left(\frac{g}{R\gamma}\right) \ln \left(\frac{T_{z_S+H}}{T_{850}}\right) \tag{7}$$

In (7) the surface pressure depends on the pressure at the reference level and the temperature profile below the reference level. If one makes the further assumption of a linear lapse rate γ_2 within the layer of topographic influence (z_S to $z_S + H$) then (7) simplifies to

$$\ln p_S = \ln p_R + \left(\frac{g}{R}\right)\left[\frac{1}{\gamma_2} \ln \left(\frac{T_S}{T_{z_S+H}}\right) + \left(\frac{1}{\gamma}\right) \ln \left(\frac{T_{z_S+H}}{T_{z_R}}\right)\right] \tag{8}$$

where $\gamma_2 = (T_{z_S} - T_{z_S+H})/H$. Note that the only dependent variable on the right hand side of (8) is T_S.

The thermodynamic energy equation (4) requires $\partial \ln p_S/\partial t$ and $\vec{\nabla}_\sigma \ln p_S$ which can be calculated by taking the local derivative and horizonal gradient of (8):

$$\frac{\partial \ln p_S}{\partial t} = \left(\frac{g}{R\gamma_2}\right) \frac{\partial T_S}{\partial t}\left[T_S^{-1} - (H\gamma_2)^{-1} \ln(T_S / T_{z_S+H})\right] \tag{9}$$

$$\vec{\nabla}_\sigma \ln p_S = \left(\frac{g}{R\gamma_2}\right) \left\{\left[T_S^{-1} - \frac{1}{H\gamma_2} \ln \left(\frac{T_S}{T_{z_S+H}}\right)\right] \vec{\nabla}_\sigma T_S \right. \tag{10}$$

$$\left. - \left[T_{z_S+H}^{-1} - \frac{1}{H\gamma_2}\ln\left(\frac{T_S}{T_{z_S+H}}\right)\right] - \frac{1}{\gamma T_{z_S+H}}\right\} \vec{\nabla}_\sigma T_{z_S+H} - \frac{g}{R\gamma T_{z_R}} \vec{\nabla}_\sigma T_{z_R}$$

8

Substituting (9) and (10) into the (4) gives the equation for the surface temperature change at a point used by the model:

$$\frac{\partial T_s}{\partial t} = - \vec{V}_s \cdot \vec{\nabla}_\sigma T_s - \vec{V}_s \cdot \vec{\nabla}_\sigma T_{z_s+H} \, (A_2 / A_1)$$

$$-\vec{V}_s \cdot \vec{\nabla}_\sigma T_{z_R} (A_3 / A_1) + Q/(A_1 C_p) + K_t A_1^{-1} \nabla_\sigma^2 T_s \tag{11}$$

where

$$A_1 = 1 - (\Gamma/\gamma_2)(1 - C_2)$$
$$A_2 = \Gamma \left[C_1 (\gamma_2^{-1} - \gamma^{-1}) - C_2 \gamma_2^{-1} \right]$$
$$A_3 = \Gamma \gamma^{-1} \left[T_s / T_{z_R} \right]$$

and

$$C_1 = T_s / T_{z_s + H}$$

$$C_2 = T_s \ln C_1 / (\gamma_2 H)$$

$$\Gamma = g / c_p$$

It is tempting to substitute (10) into the pressure gradient force term of the momentum equation (1). However, such a substitution would leave the pressure gradient term as a small difference between two large terms of opposite sign, namely $- g\vec{\nabla}_\sigma z_s$ and $- RT_s \vec{\nabla}_\sigma \ln p_s$. Since both of these terms are approximated by finite differences, which possess some truncation error, their difference would be a poor estimate of the pressure gradient force. Since most of horizontal variation of surface pressure results from the hydrostatic effects of surface height changes, it is useful to calculate the horizontal pressure gradient force so that the hydrostatic variations are removed before the finite difference approximations are made. This can be done by first differentiating (5) using the General Leibnitz Rule for differentiating integrals:

$$\vec{\nabla}_\sigma \ln p_s = (\tfrac{g}{R}) [T_{z_R}^{-1} \vec{\nabla}_\sigma z_R - T_s^{-1} \vec{\nabla}_\sigma z_s - \int_{z_s}^{z_R} T^{-2}(z) \, \vec{\nabla}_\sigma T(z) dz] \tag{12}$$

9

Substituting (12) into the pressure gradient force term of the momentum equation gives

$$g\vec{\nabla}_\sigma z_s + RT_s \vec{\nabla}_\sigma \ln p_s = g[(T_s/T_{z_R})\vec{\nabla}_\sigma z_R - T_s \int_{z_s}^{z_R} T(z)\vec{\nabla}_\sigma T(z)dz \qquad (13)$$

Note that during the manipulation to produce (13) the large hydrostatic term $g\vec{\nabla}_\sigma z_s$ is explicitly cancelled so that the hydrostatic variation of pressure along the $\sigma = 1$ surface has been removed.

Since the vertical temperature structure in the model is specified and therefore known, the second term of (13) can be explicitly integrated. Thus,

$$g\vec{\nabla}_\sigma z_s + RT_s \vec{\nabla}_\sigma \ln p_s = g[(e_1 - H/T_{z_s} + H)\vec{\nabla}_\sigma T_s$$
$$-(e_1 + (e_2/\gamma)(T_{z_s} + H^- T_{z_R})\vec{\nabla}_\sigma T_{z_R} + (\gamma e_1 - e_2 + 1)\vec{\nabla}_\sigma z_s \qquad (14)$$
$$+ (e_2 - \gamma e_1)\vec{\nabla}_\sigma z_R]$$

where

$$e_1 = (T_s \gamma_2^{-1})(T_{z_s}^{-1} + H \quad - (H\gamma_2)^{-1} \ln(T_s/T_{z_s} + H))$$
$$e_2 = T_s/T_{z_s} + H$$

Substituting the pressure gradient force term (14) into the momentum equation (1) eliminates the last explicit reference to surface pressure. Equation (1), with the substitution of (14), and (11) now form a closed pair of equations in the variables $\vec{V}_s$ and T_s. If needed, the surface pressure can be diagnosed from (7) once T_s is known.

b. Diabatic Heating

In order to accurately model the mesoscale flow in complex terrain it is usually necessary to include the effects of surface heating or cooling and the resulting thermally induced circulations. In this model the surface diabatic forcing is parameterized by including a heating/cooling term Q/c_p in the thermodynamic energy equation (4). In each model run the land and water values of the diabatic forcing term are assigned by examining actual surface temperature changes. For each diabatic forcing run the model is first integrated to a steady state without the diabatic effects. This is followed by a six hour run including the heating or cooling.

Let us consider how the model's diabatic forcing produces sea/land breezes and mountain/valley or slope winds. In the case of a sea breeze, greater heating over land produces larger temperature increases there than over water. This results in larger hydrostatic pressure falls over land than water which creates an onshore pressure gradient force (see Eq. 14) that produces a sea breeze. The opposite occurs at night when greater cooling (Q<0) over land produces an offshore flow or land breeze.

The model's production of valley or upslope winds can be explained by referring to Fig. 2. In this picture we assume that uniform heating occurs in a layer of depth H in which the lapse rate is γ_H. Above this layer an environmental lapse rate of γ occurs. Points A and B are both at the same height. With heating in the surface layer the pressure will fall at B but not at A since none of the air above A is being warmed. The result will be a horizonal pressure gradient directed from
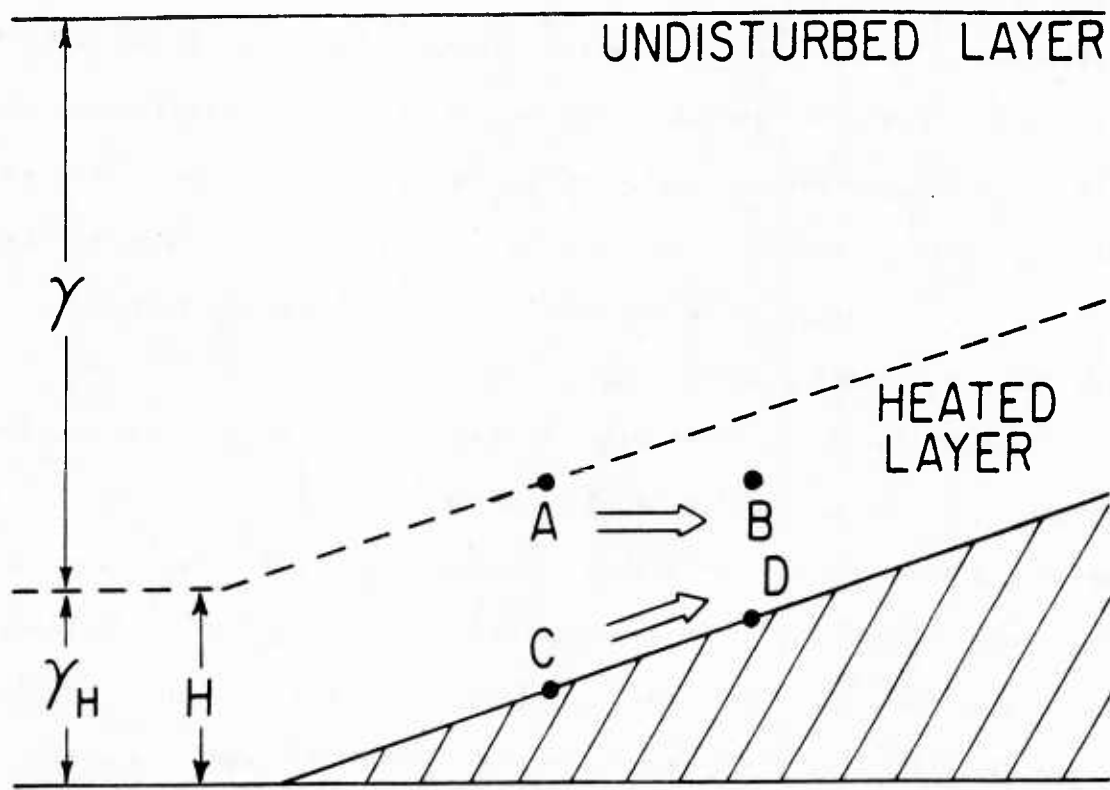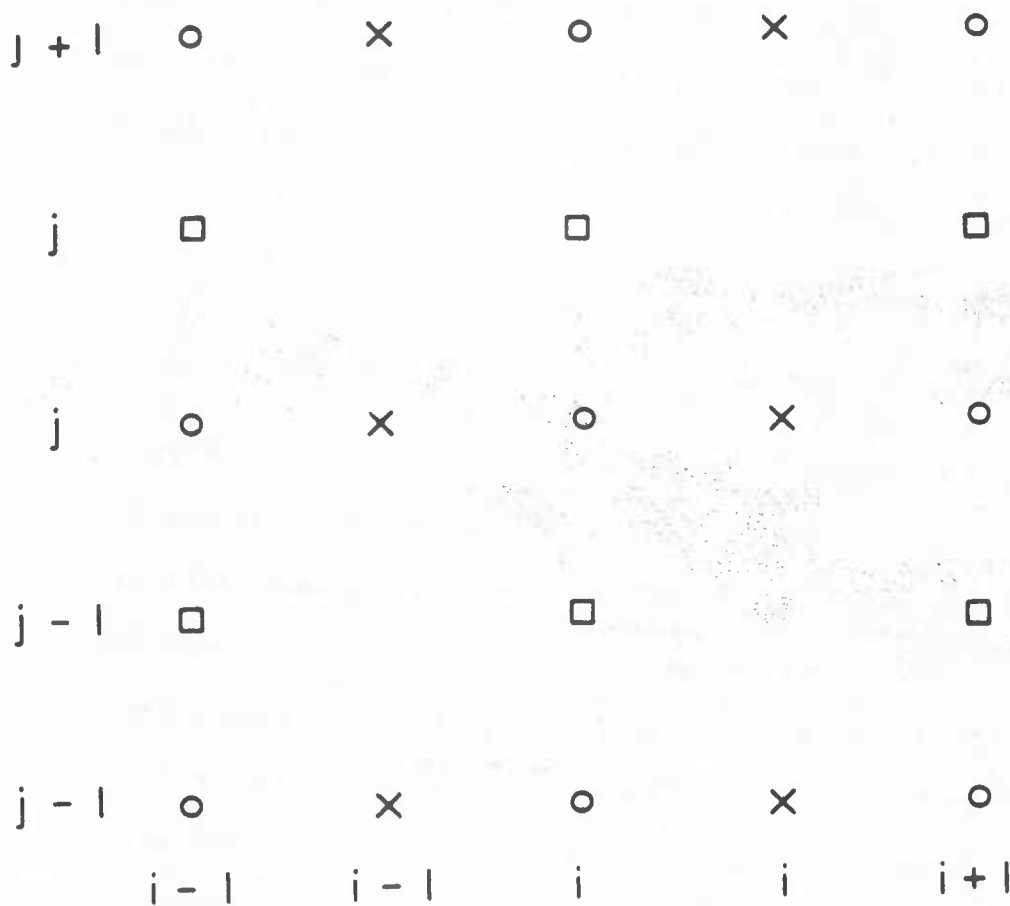
11

Figure 2.   Schematic of a heated slope.

A to B or towards greater elevation. If the pressures at points A and B are then reduced hydrostatically through the uniformly heated layer to points C and D on the surface there will be a pressure gradient force (with the hydrostatic component removed) towards higher elevation. This mechanism for the production of upslope flow also exists in the model; in fact, the model structure (Fig. 1) is quite similar to the picture shown above.

c. Numerical Methods

For the cases presented in this paper, the reference pressure level was taken to be 850 mb. At this level, temperatures and geopotential heights were interpolated from the appropriate National Meteorological Center (NMC) analysis to the model grid. Using vertical sounding data from the closest upstream radiosonde, a free atmospheric lapse rate was found. This lapse rate was used with the 850 mb temperature and height data to establish a surface temperature field. The initial wind field was then computed by balancing the initial surface pressure-gradient, coriolis and frictional forces. Appendix III gives details of the initialization.

The model variables were positioned on an Arakawa "C" staggered grid (Mesinger and Arakawa, 1976) as shown in Fig. 3. Such a grid is convenient for finite differencing and reduces truncation error. All of the runs presented in this paper were made on a 74 by 75 point grid using a resolution of approximately 7.5 km.

After testing several time integration schemes it was found that a modified second-order Adam's-Bashforth scheme was most stable.

13

j + l   o   x   o   x   o

j   □   □   □

j   o   x   o   x   o

j - l   □   □   □

j - l   o   x   o   x   o

        i - l   i - l   i   i   i + l

LEGEND: o   T, z

                x   U

                □   V

Figure 3.   Model grid structure.

Specifically, we used:

$$\phi^{(n+1)} = \phi^n + \frac{\Delta t}{2} \left[3 \frac{\partial \phi}{\partial t}^{(n)} - \frac{\partial \phi}{\partial t}^{(n-1)} \right]$$

where ϕ is any dependent variable, Δt is the time step, and n+1, n and n-1 represent the next, current and previous times. For all model runs a time step of 180 s was used.

After initialization, the model was integrated to steady state, i.e., until the domain-averaged tendencies of the wind components ($\partial u_s / \partial t$ and $\partial v_s / \partial t$) dropped below a specified small value ($10^{-6} m\ s^{-2}$). Using this convergence criterion and a 74 by 75 grid, the model ran in 30 s on the CRAY 1 at the National Center for Atmospheric Research (NCAR). By reducing the grid size or by using a less strict convergence criterion, run time can be drastically reduced.

Surface temperatures are fixed at inflow boundaries but are allowed to vary at outflow boundaries. Wind components are allowed to vary on all boundaries. To compute $\partial \vec{V}_s / \partial t$ and $\partial T_s / \partial t$ on the boundaries it is necessary to assume values of T_s, u_s and v_s just outside the model boundary. Tests of several possibilities indicated that the best assumption is

$$u_s(B - 1) = u_s(B + 1)$$
$$v_s(B - 1) = v_s(B + 1)$$
$$T_s(B - 1) = T_s(B + 1)$$

where B + 1 and B - 1 signify one grid length inside and outside a boundary, respectively.

The advection terms in the momentum equations are finite differenced in space according to Gerrity et. al. (1971) while the momentum diffusion terms are differenced following Danard (1971).

15

Temperature advection was center-differenced and the temperature diffusion terms followed Danard (1971) except that temperatures surrounding each point were first adjusted to the same elevation using their respective local lapse rates (see Appendix II).

3. Model Simulations

The three models were run for three test areas.

a) A section of the Pacific Northwest that encompassed southwestern British Columbia, western Washington State and northwestern Oregon (Fig. 4). This domain is nearly ideal for testing mesoscale models for use in complex terrain since there exists substantial topographic relief and land/water contrast and a large amount of surface data for evaluation of results. Furthermore, several recent studies (e.g., Mass, 1981, 1982; Overland and Walter, 1981; Walter and Overland, 1982; Reed 1981, 1982) provide much observational knowledge of the mesoscale low-level flow of the region. The main features of the domain include the north-south oriented Cascade mountains, which reach heights exceeding 2000 m and substantially block low-level flow, a parallel coastal range of somewhat lower heights to the west with several low-level gaps, a lowlands area between the two mountain ranges encompassing Puget Sound and the Strait of Georgia, and the Pacific Ocean to the west. Figure 5 shows the topography used for this test area. The model coastline shown in this figure represents the 30 m height contour.

b) A region around San Francisco Bay with the Pacific Ocean to the west and the Sierra Nevada Mountains to the east (Fig. 6). This domain has far less severe terrain than (a).

c) The region around the Subic Bay Harbor (Fig. 7).

16

Figure 4.   Major geographical features of the model domain.
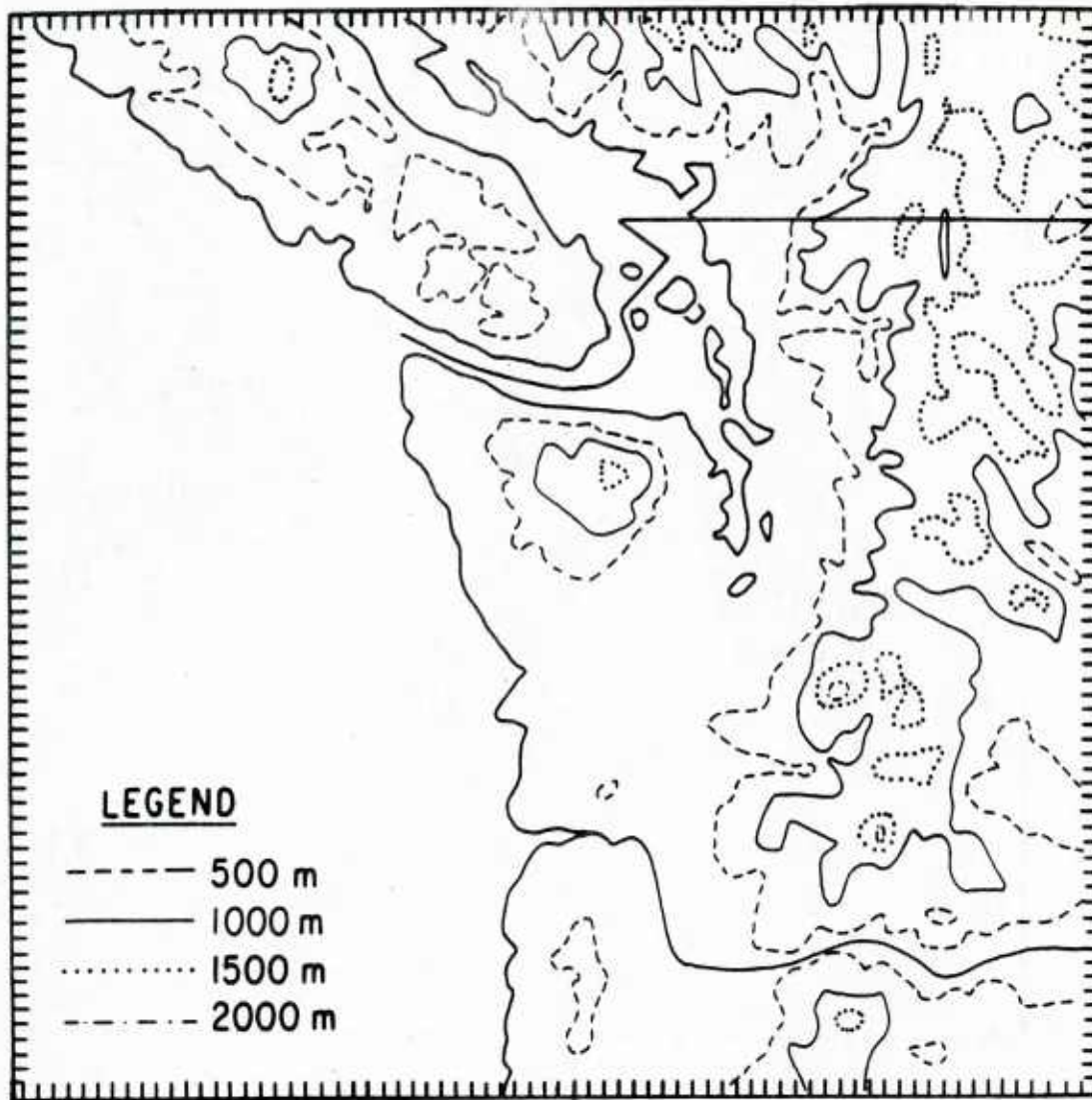
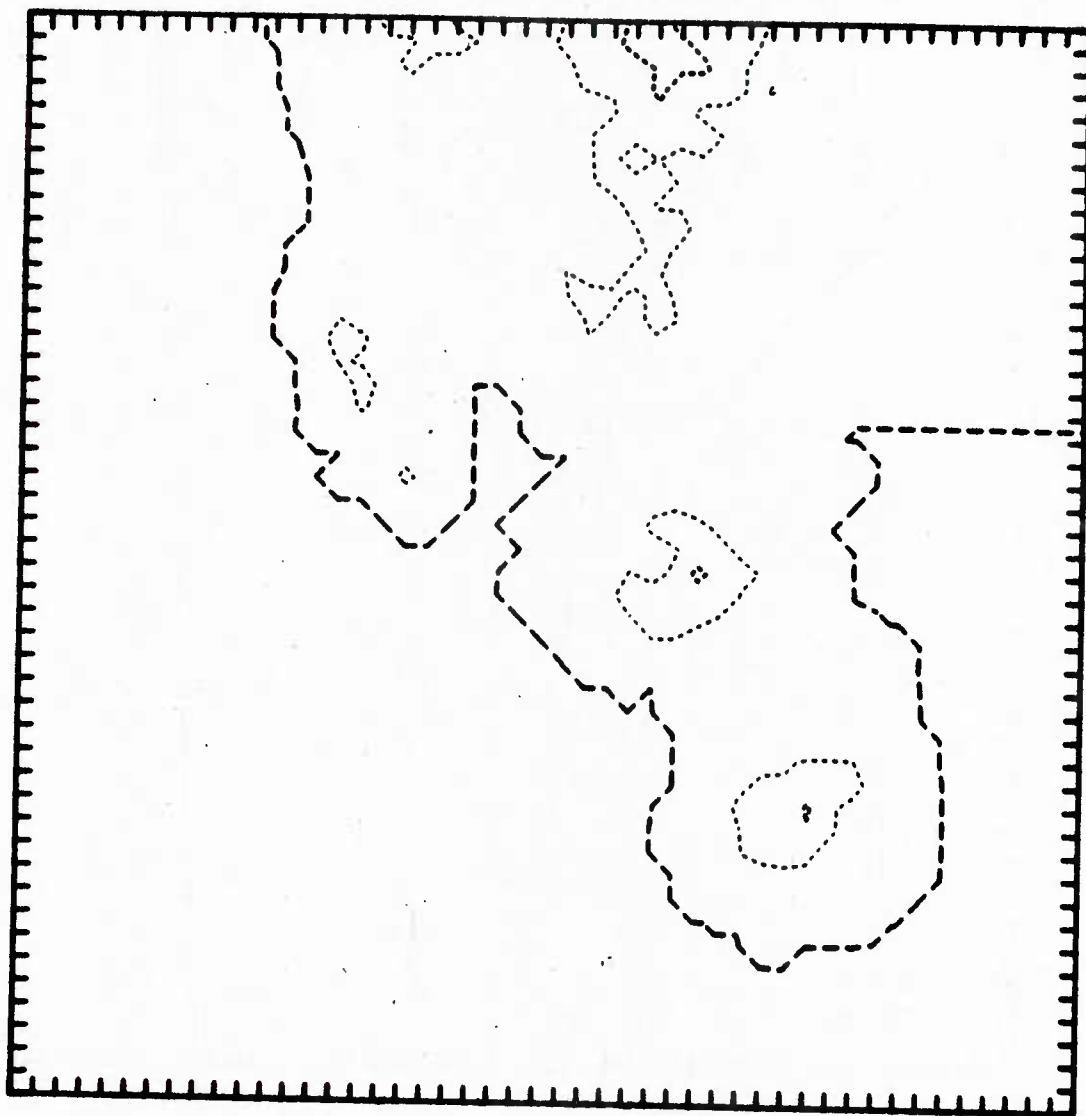Figure 5. Topography used in the model runs.

Figure 6. Model topography for San Francisco Bay area runs. Contours every 500 m.
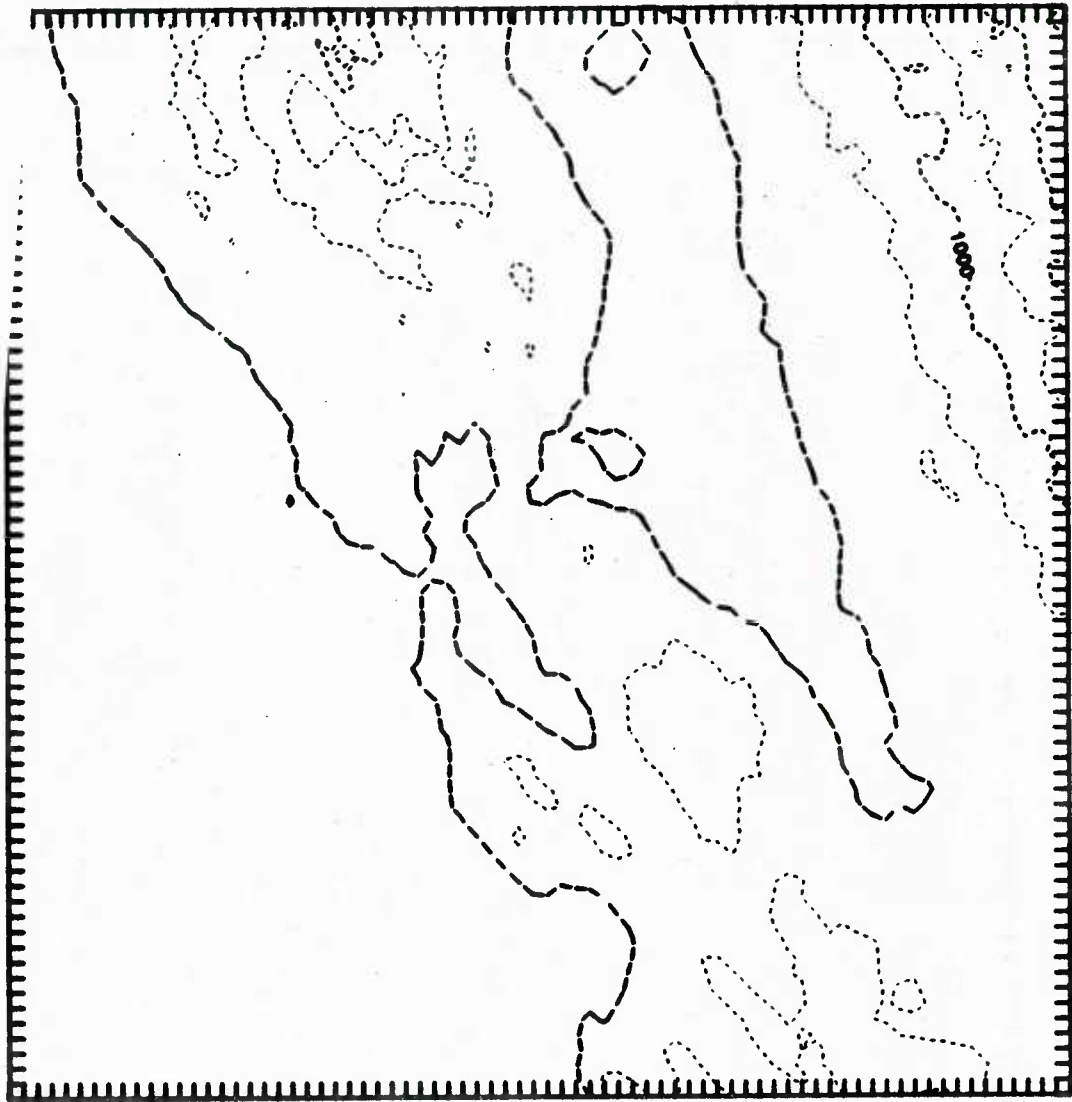
Figure 7.   Model topography for Subic Bay runs.   Contours every 500 m.

The following sections will describe model runs that include synoptic scale flows of various directions, lower-tropospheric stabilities and magnitudes of diabatic forcing for the above three areas. Diabatic heating was only available in the Mass-Dempsey model. With some effort it could be added to the mixed layer model. There is no way to realistically add diabatic heating to the mass conservation model.

a. Western Washington Domain

   A. May 3, 1978 at 00 GMT: Northwesterly large scale flow and strong heating.

In the 24 hours before the verification time of this case a cold front had moved eastward from the Pacific into eastern Washington State (Fig. 8a). The surface winds at well-exposed coastal stations, representative of low-level, synoptic-scale flow, veered from south-southwest to west-northwest with frontal passage. Similarly, the 850 mb flow on the coast veered from west-southwest at 00 GMT on May 2 to the northwest at 00 GMT on May 3 (Fig. 8b). The sounding at the closest upstream station, Quillayute, WA., on the Washington coast, is shwon in Fig. 8c. A superadiabatic layer, caused by surface heating, is noted at low levels with the weakly stable layer above topped by an inversion at 860 mb. Above 850 mb the sounding becomes quite stable. Figure 8d shows a detailed meso-scale picture of the surface flowfield at the verification time of the model run. An interesting feature is the channeling of the flow north and south of the Olympic Mountains, its deflection by the Cascades and the resulting horizontal convergence in Puget Sound. (Note the calm wind in the southern Sound between the northerly and southerly flows). This phenomenon, termed the Puget Sound Convergence Zone, is a significant weather feature of the area and is often associated with an east-west band of cloudiness and precipitation across Puget Sound (Mass, 1981).
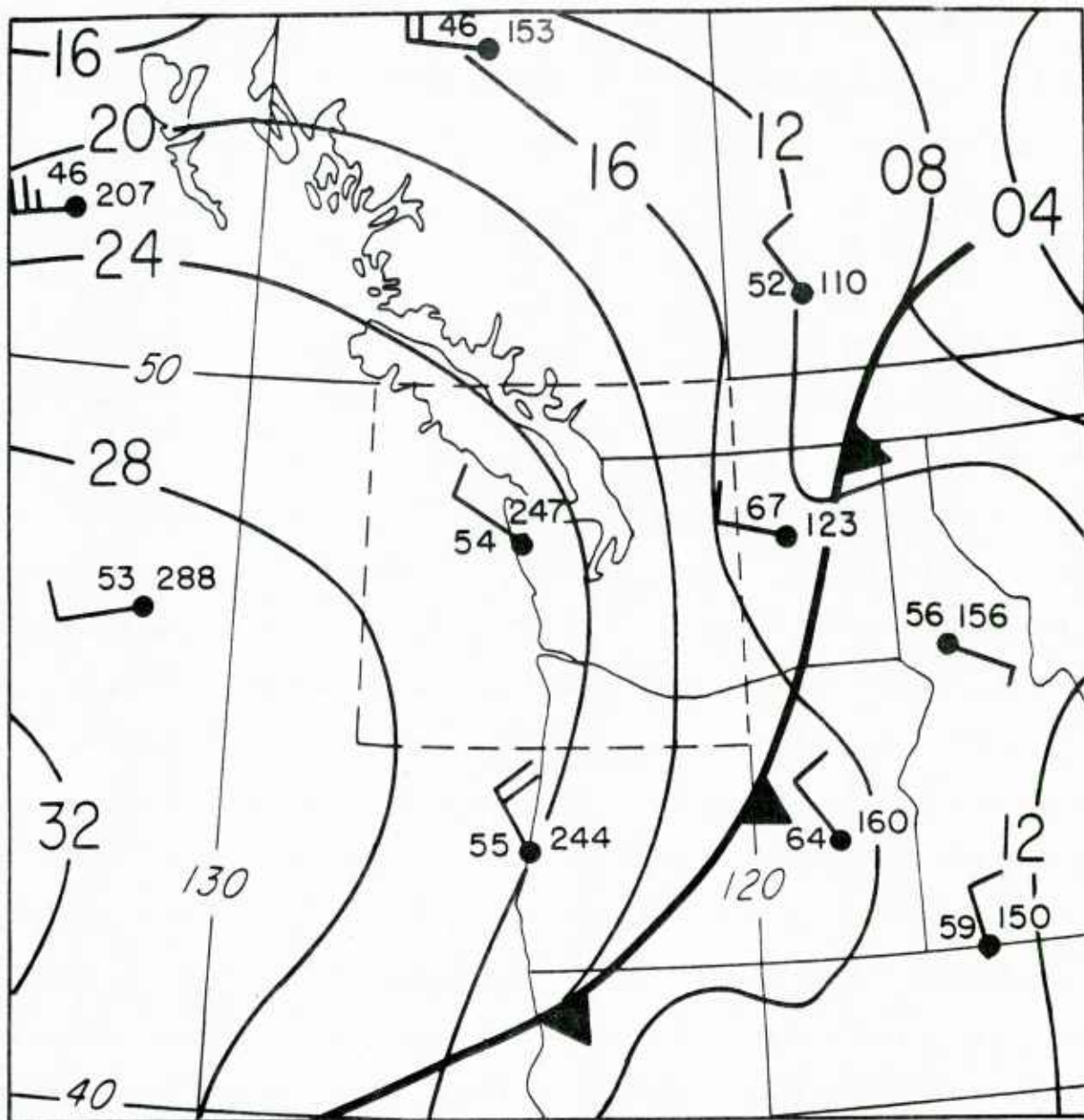
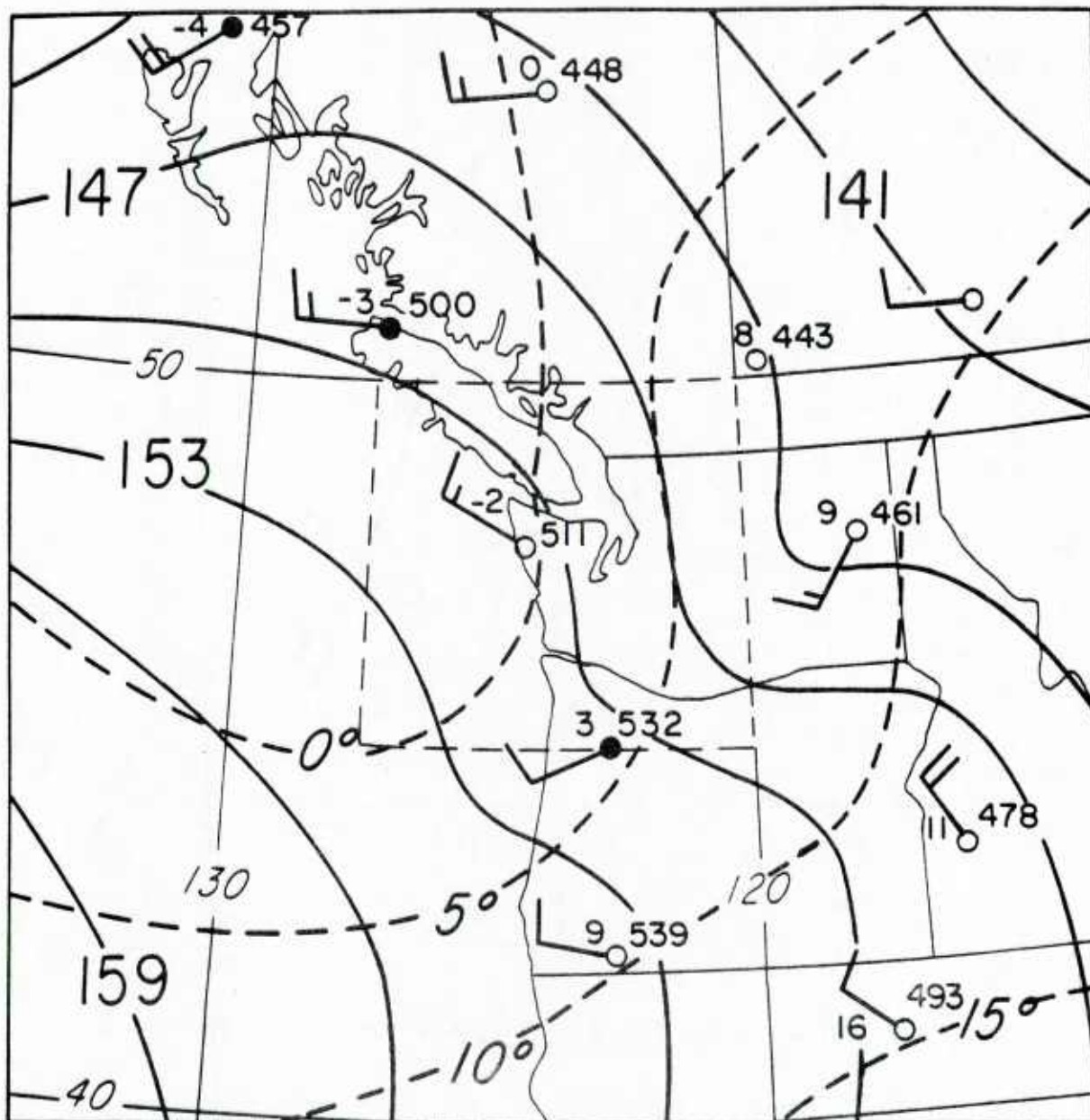Figure 8a. Run for 3 May 1978, 00 GMT, surface chart.

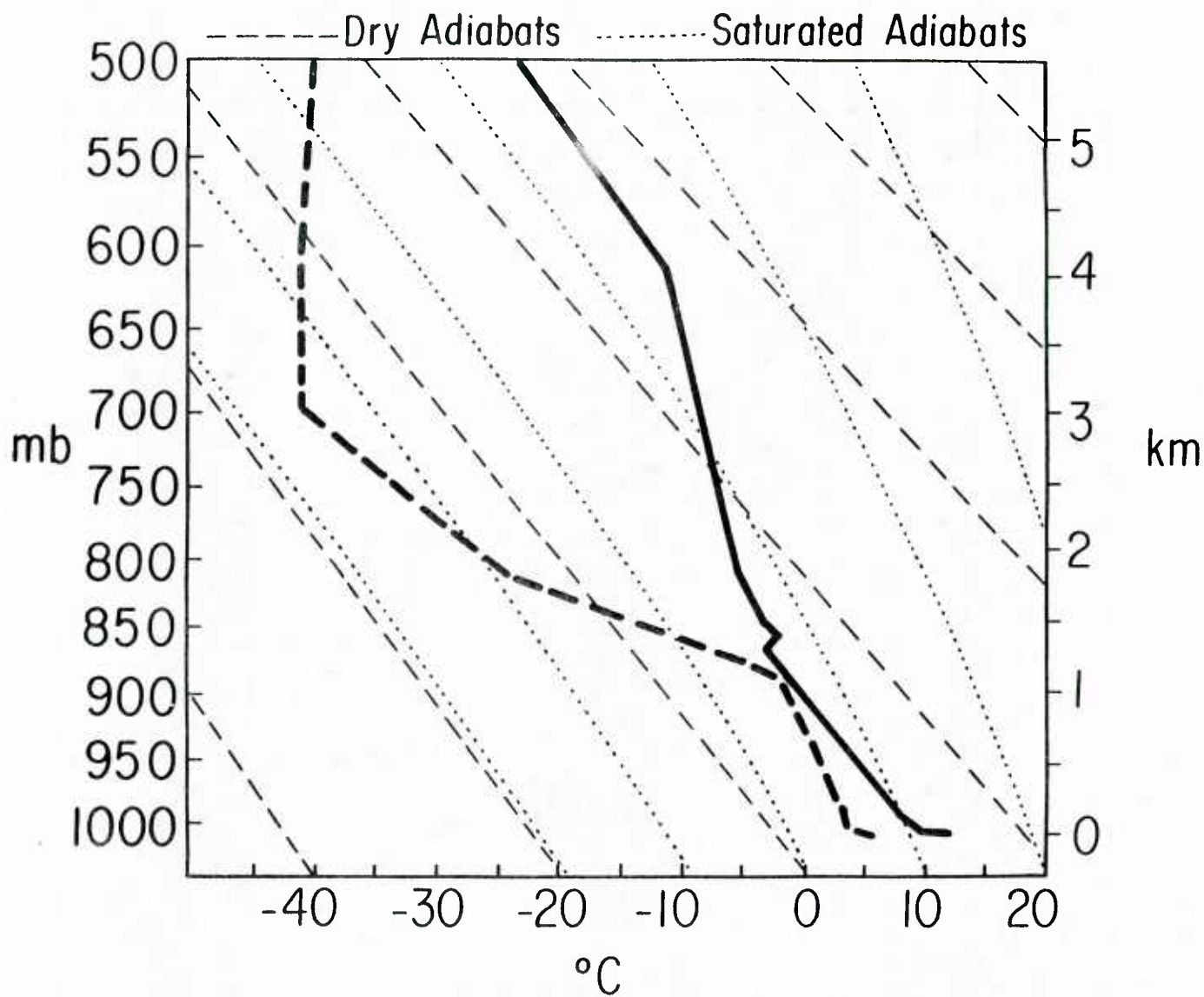Figure 8b. Run for 3 May 1978, 00 GMT, 850 mb chart.

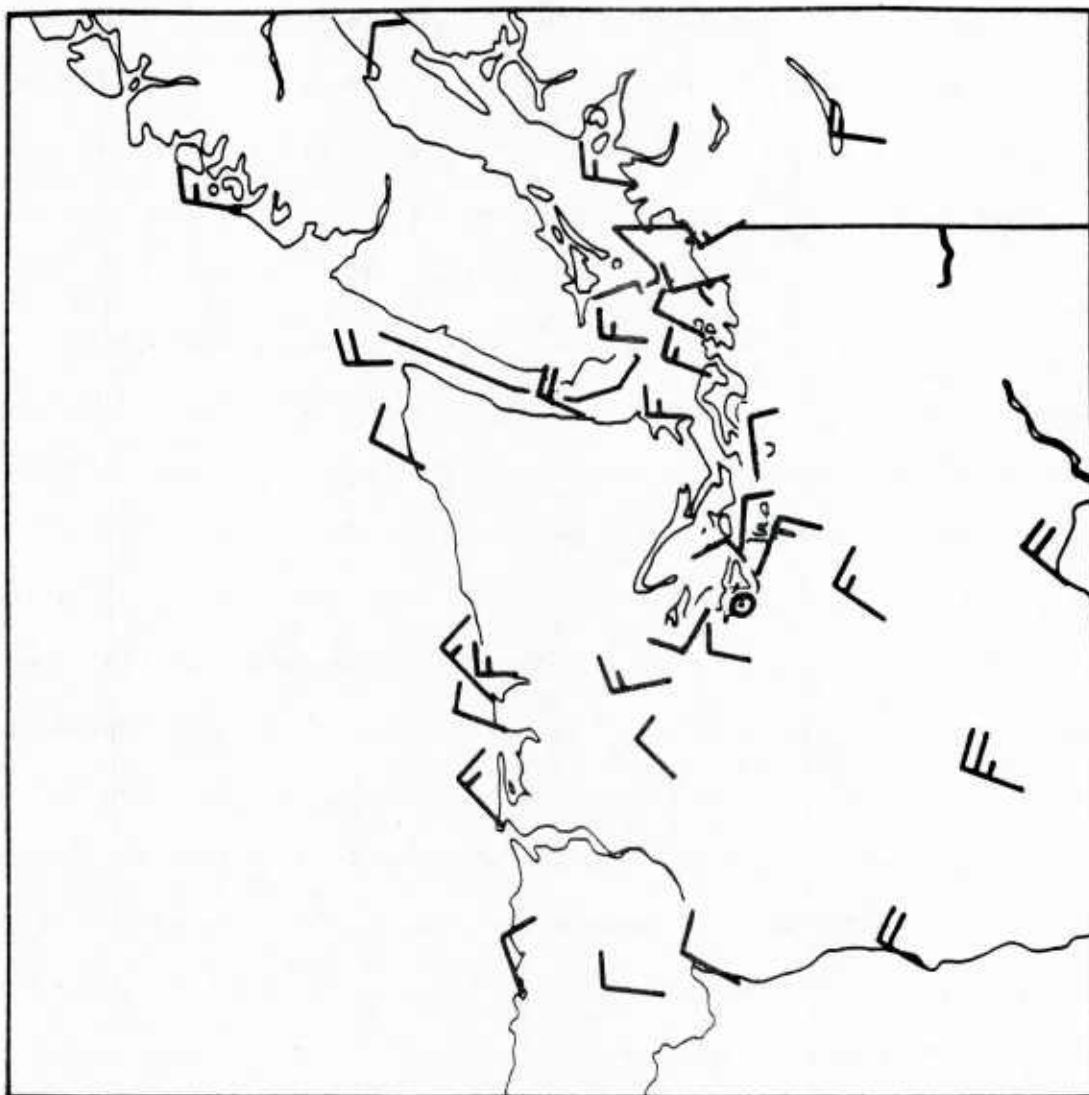Figure 8c. Run for 3 May 1978, 00 GMT, sounding at Quillayute, WA.

Figure 8d. Run for 3 May 1978, 00 GMT, observed surface winds.

1. <u>Mass-Dempsey Model.</u>

The model, run to a steady state without any surface diabatic heating or
cooling, produced the surface wind field[2] shown in Fig. 8e. These model winds
show that the northwesterly flow at the coast is deflected north and south around
the Olympics with a zone of confluence and convergence in northern Puget Sound.
This convergence is substantially north of the actual location shown in Fig. 8d.

From previous studies (Staley, 1956; Mass, 1982) we know that diurnal
circulations are an important component of the low-level wind field in this region,
particularly during the warm months from April through October. For example,
daytime heating over land pulls air towards the Puget Sound basin through the
Strait of Juan de Fuca and results in northerly flow moving into the Sound. To
include this and other thermally forced diurnal effects, a surface diabatic heating
rate of 9°C per 6 hr over land and 2°C per 6 hr over water was included and the
model was run for an additional 6 hours. The resulting surface wind field is
shown in Fig. 8f. As in the real world, surface heating resulted in greater flow
into the Strait of Juan de Fuca and the enhancement of northerlies in Puget Sound.
In addition there is enhanced upslope and onshore flow throughout the domain.
Significantly, the surface convergence line has moved southward to a position just
a few km to the north of the observed location. Thus, it appears that given the
proper synoptic scale and diabatic forcings, the model is able to correctly
diagnose the existence and position of this important mesoscale feature. Also
note that with diabatic heating the model was able to correctly indicate southward
flow in the northern Strait of Georgia, southwesterly flow south of Vancouver,
B. C. and northwesterly flow on the Washington coast and around Portland, Oregon.

---

[2]Note that the vector plots of the surface wind show every other vector,
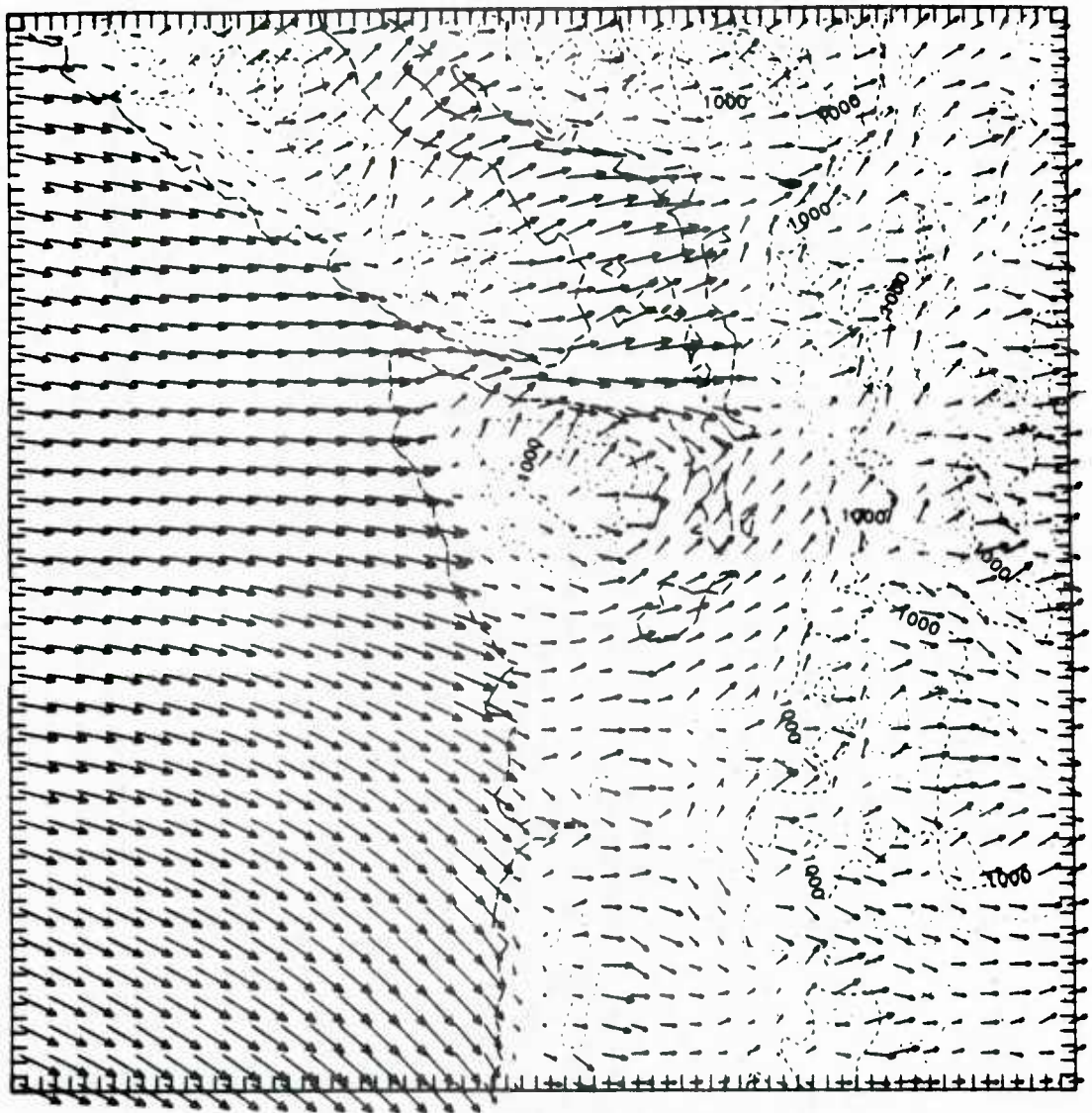rather than all vectors, in the domain for greater clarity of presentation.

26

Figure 8e. Run for 3 May 1978, 00 GMT, model surface winds
without diabatic forcing.

Figure 8f. Run for 3 May 1978, 00 GMT, model surface winds with diabatic heating.

The model and observed sea level pressure fields (not shown) have similar configurations; both possess a narrow pressure trough directed southeast-northwest over Puget Sound in the area of surface convergence and a narrow pressure ridge along the Strait of Juan de Fuca.

2.   Mixed Layer Model

The output of a run of the mixed layer model (without heating) is shown in Fig. 9. Northwesterly flow on the coast is deflected around the Olympics with both branches turning towards the northeast by the Cascades. Unlike the Mass-Dempsey model there is no tendency for northerlies in upper Puget Sound. Light winds occur to the lee of the Olympics. One notes eratic, unphysical high winds on some of the lateral boundaries.

3.   Mass Conservation Model

These results (Fig. 10) evince little deflection by the topography of the region.

B.   November 23, 1982 at 12 GMT: East-northeasterly large scale flow with moderate diabatic cooling.

The surface synoptic pattern at this time was dominated by a cold, high pressure system centered to the northeast of the model domain with low pressure over the Pacific to the southeast (Fig. 11a). This pattern is relatively unchanged at 850 mb (Fig. 11b). The upstream sounding at Spokane in eastern Washington State (Fig. 11c) indicates a very stable lower troposphere with a surface based inversion to 890 mb, with nearly isothermal conditions above.

1.   Mass-Dempsey Model.

The detailed observed mesoscale surface windfield (Fig. 11d) shows easterly winds on the Washington coast, northerlies in northern and central Puget Sound
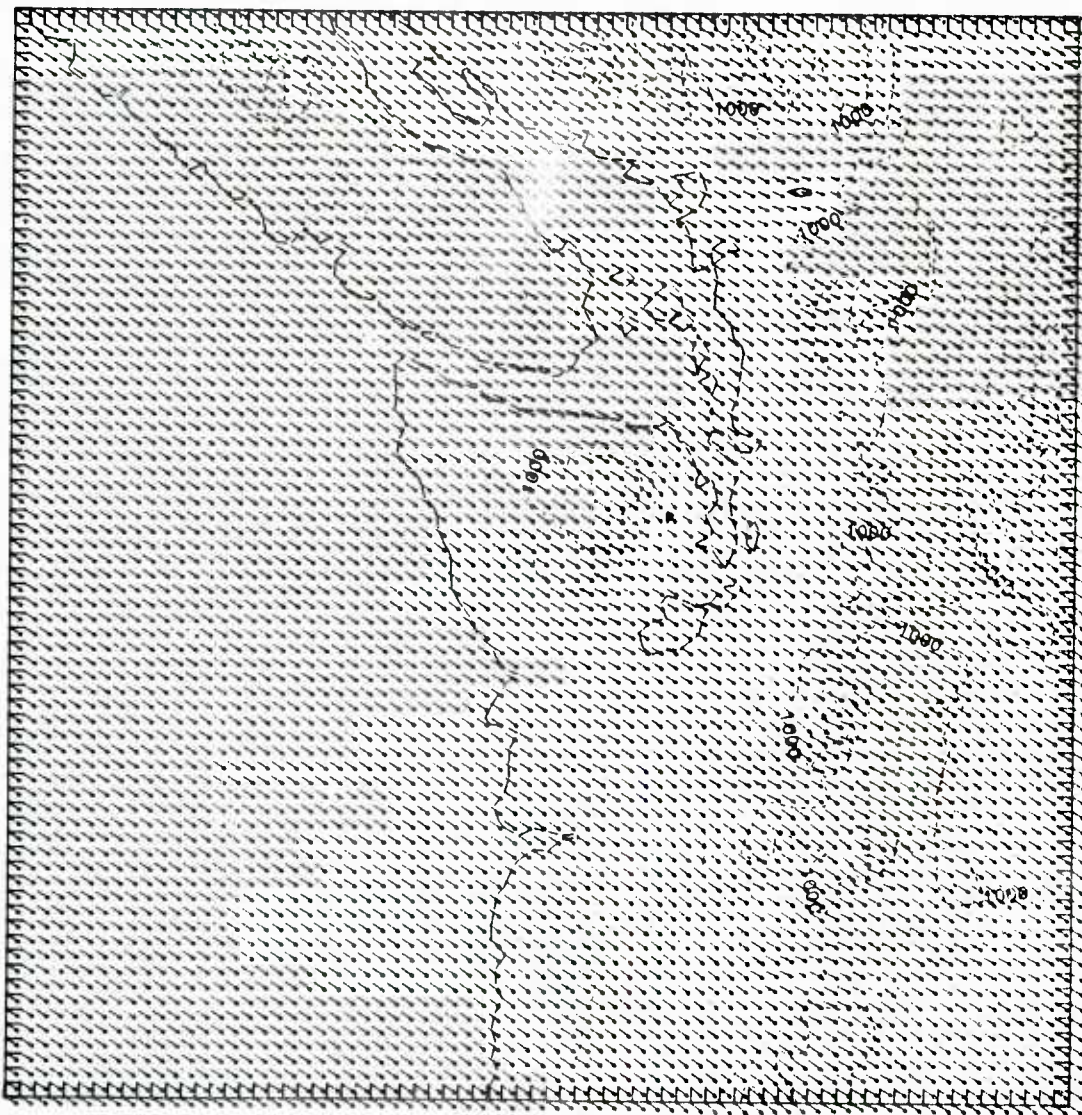
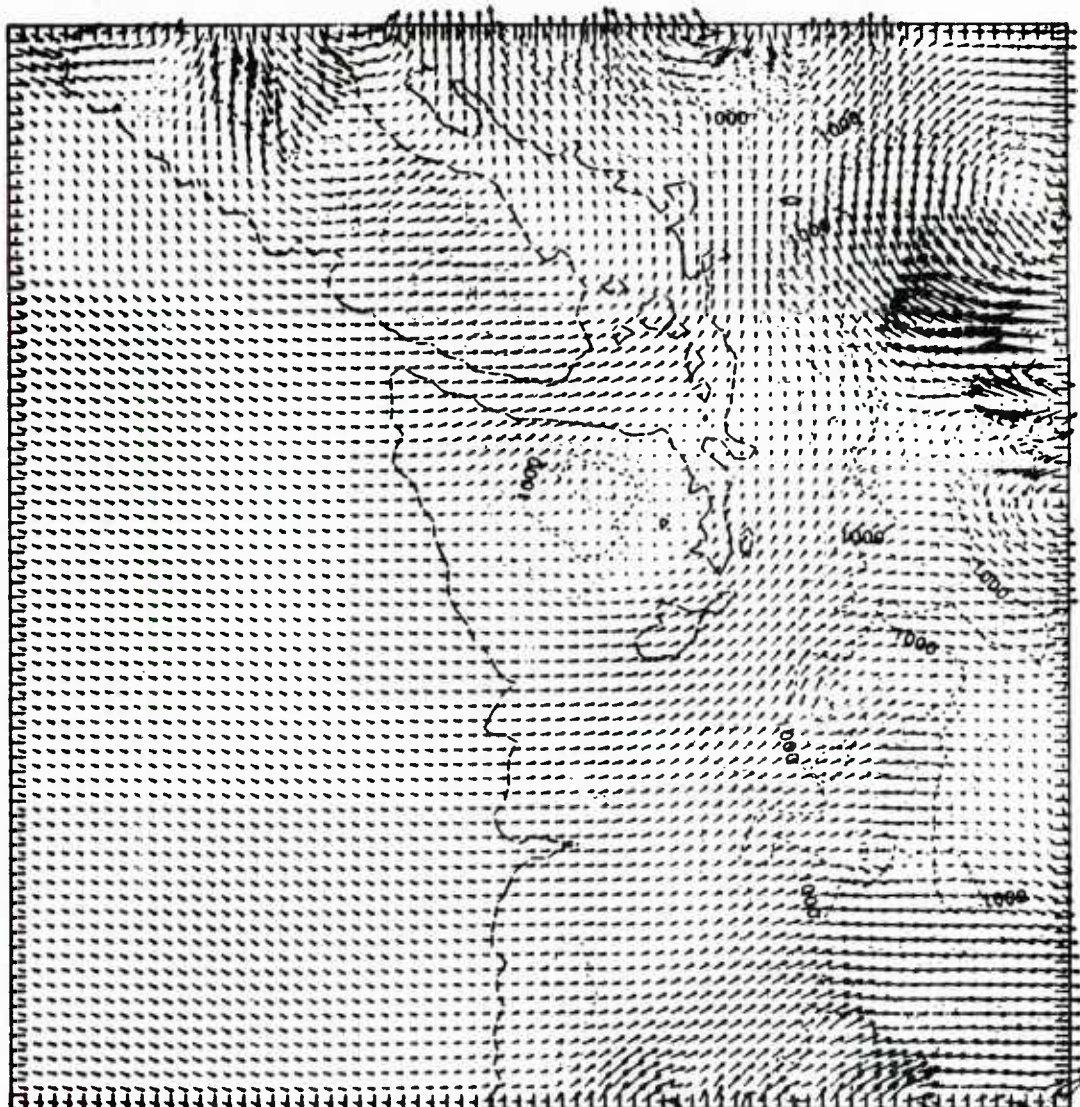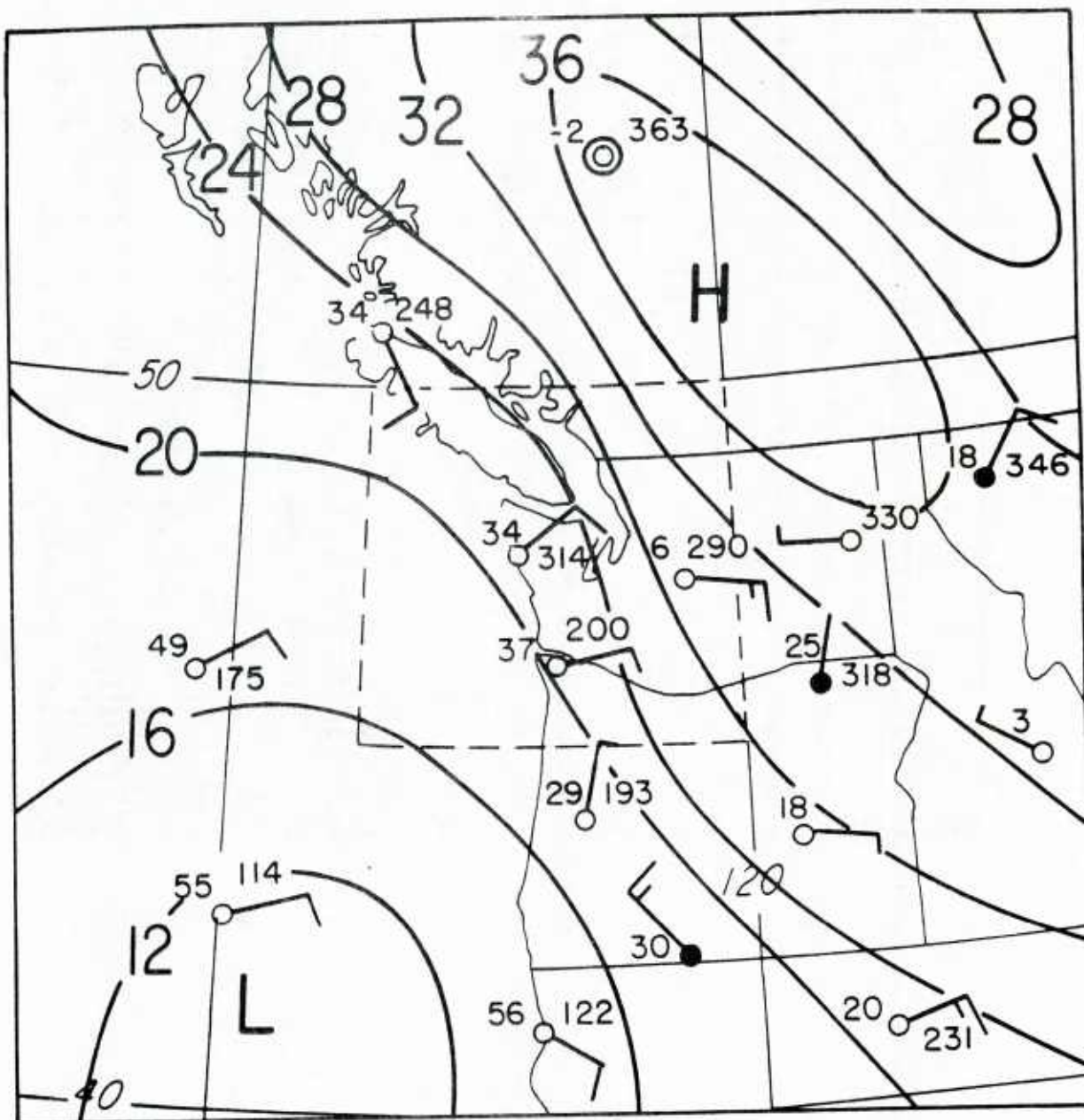Figure 9.   Mass conservation model wind field for May 3, 1978 at 00 GMT.
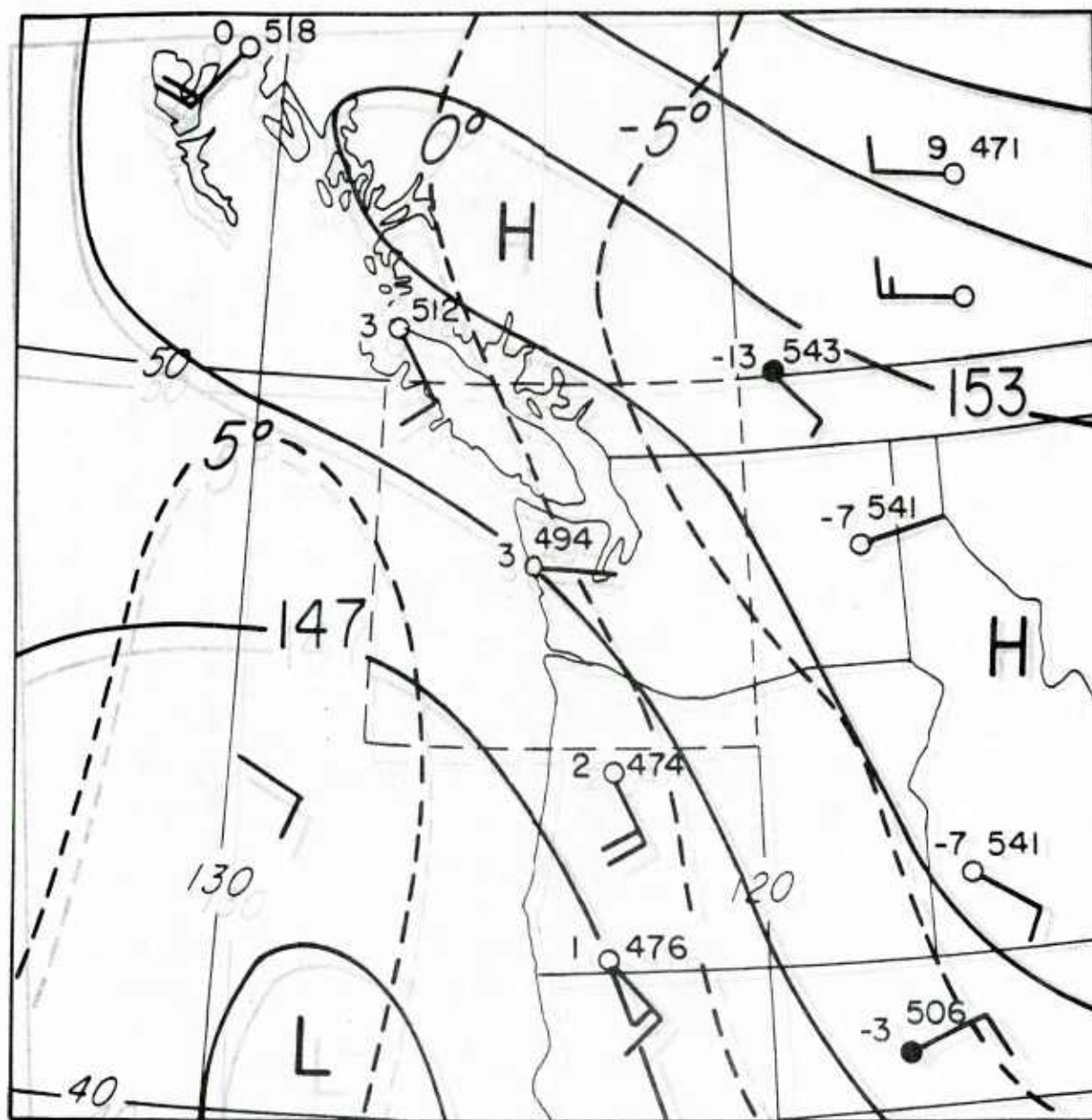
Figure 10. Mixed layer model wind field for May 3, 1978 at 00 GMT.

Figure 11a. Run for 23 November 1982, 12 GMT, surface chart.

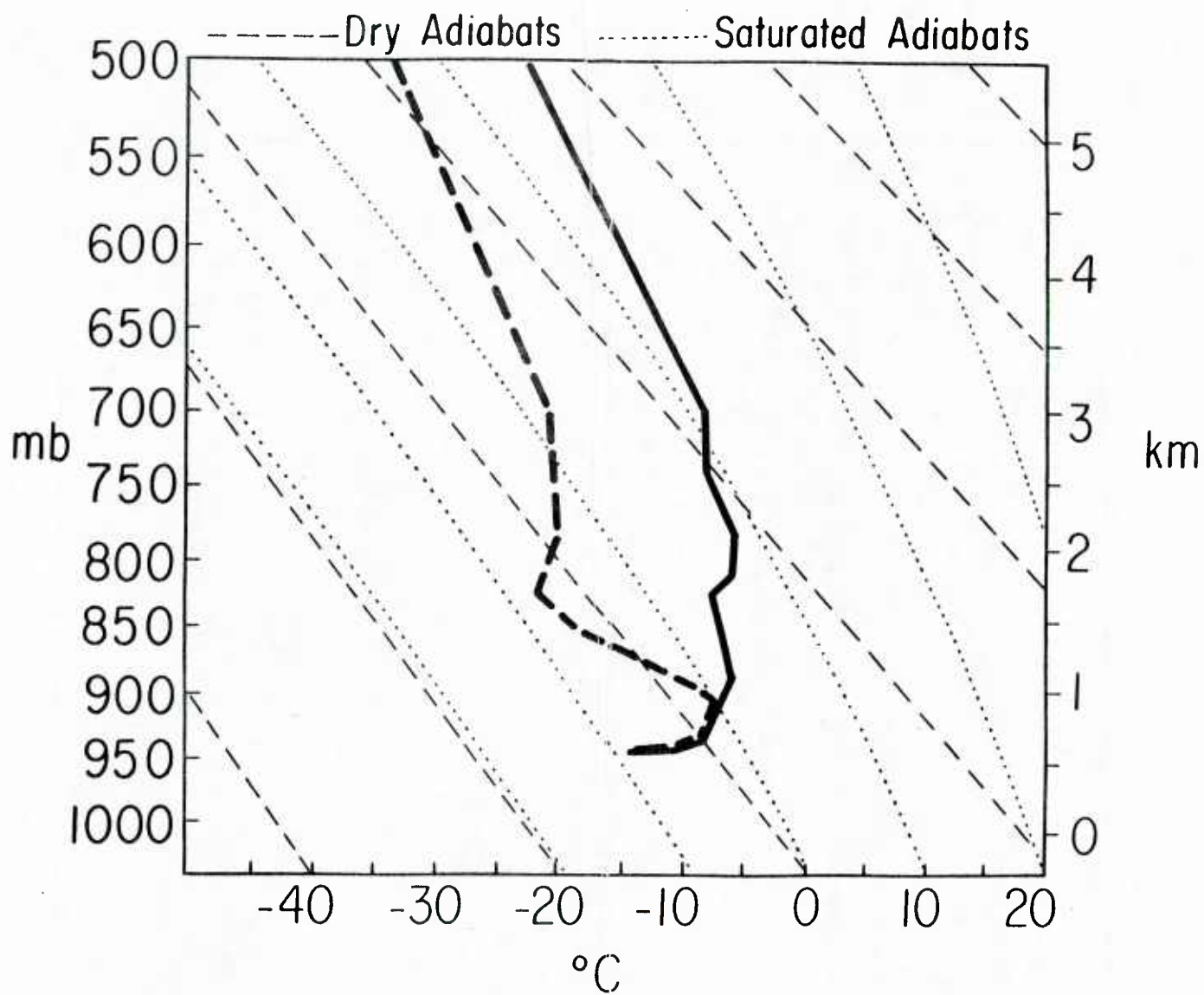Figure 11b. Run for 23 November 1982, 12 GMT, 850 mb chart.

33

Figure 11c. Run for 23 November 1982, 12 GMT, sounding at Spokane, WA.

and calm winds in the southern Sound. Cold air appears to be draining towards the center of the Strait of Georgia with easterlies on the western side and westerlies on the eastern side. Figure 11e shows a model run that included 6 h of cooling at a rate of 5°C per 6 h over land and 1°C per 6 h over water. There are many similarities and some differences with the actual wind field. Note that like the observed winds the model shows northeasterly flow on the north Washington coast while to the south the winds switch to southeasterly and then northeasterly. Winds in northern and central Puget Sound are from the north-northeast and become nearly calm in the southern Sound as observed. The model did not reproduce the observed weak southwesterlies caused by blocked flow on the northeast side of the Olympic Mountains or the westerly drainage flows on the eastern side of Vancouver Island. An interesting flow pattern produced by the model is the east-west line of confluence in the lee of the Olympic Mountains. Although we lack the surface observations to directly verify this feature, in similar situations in which the offshore flow is sufficiently cold to form convective cloudiness over the warmer water, it is observed that an east-west band of low-clouds stretching from just offshore from the Olympics is found. Clearly, this band is created by the linear confluence-convergence feature forced by the Olympics and duplicated in the model.

   2. Mixed layer model blew up. Mass conservation model not run.

   C. December 17, 1982 at 12 GMT: Southerly large scale flow with weak diabatic cooling.

   1. Mass-Dempsey Model.

The surface synoptic pattern at this time (Fig. 12a) shows a relatively deep low center to the northwest of the domain with a trailing occluded front that
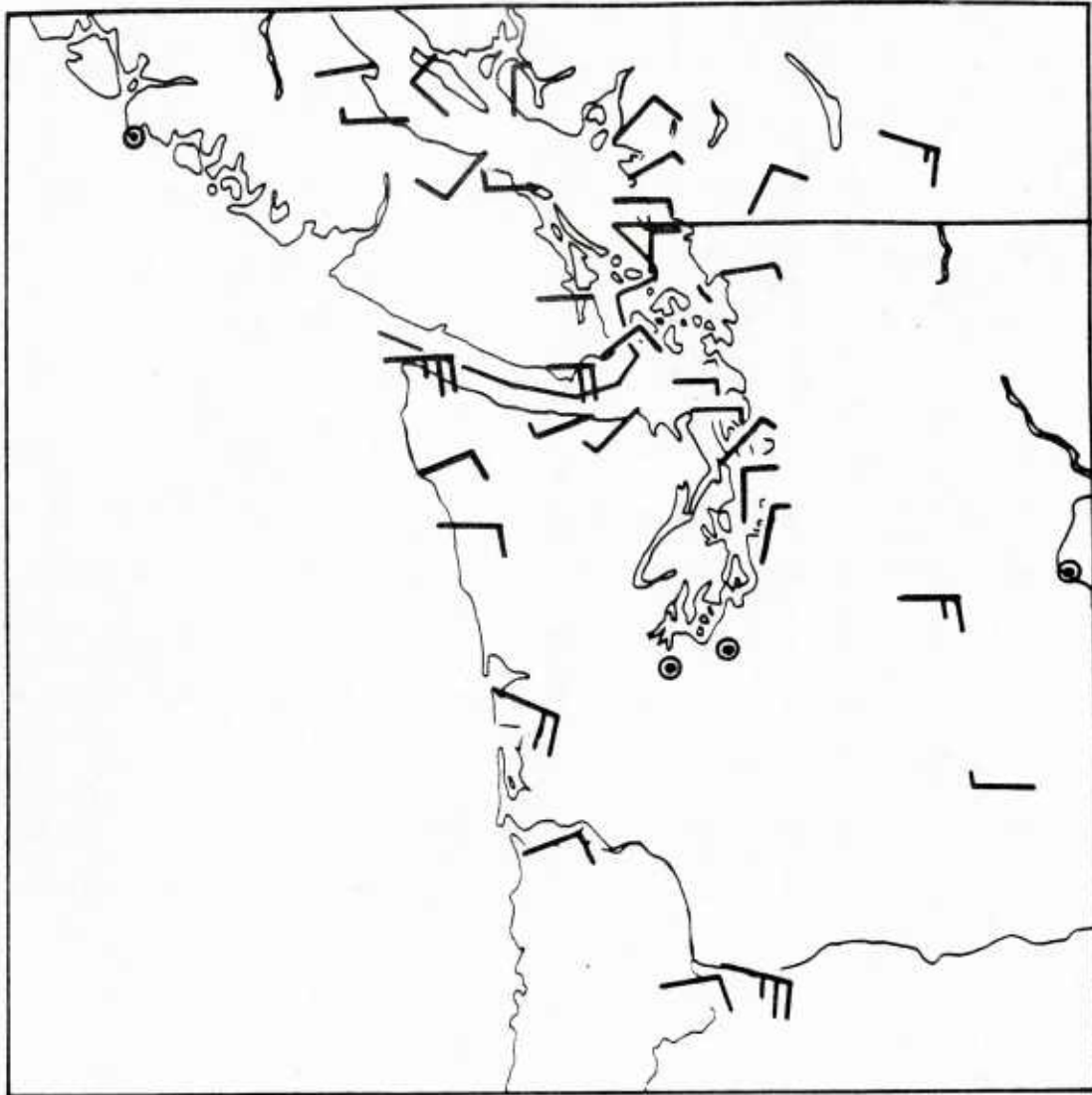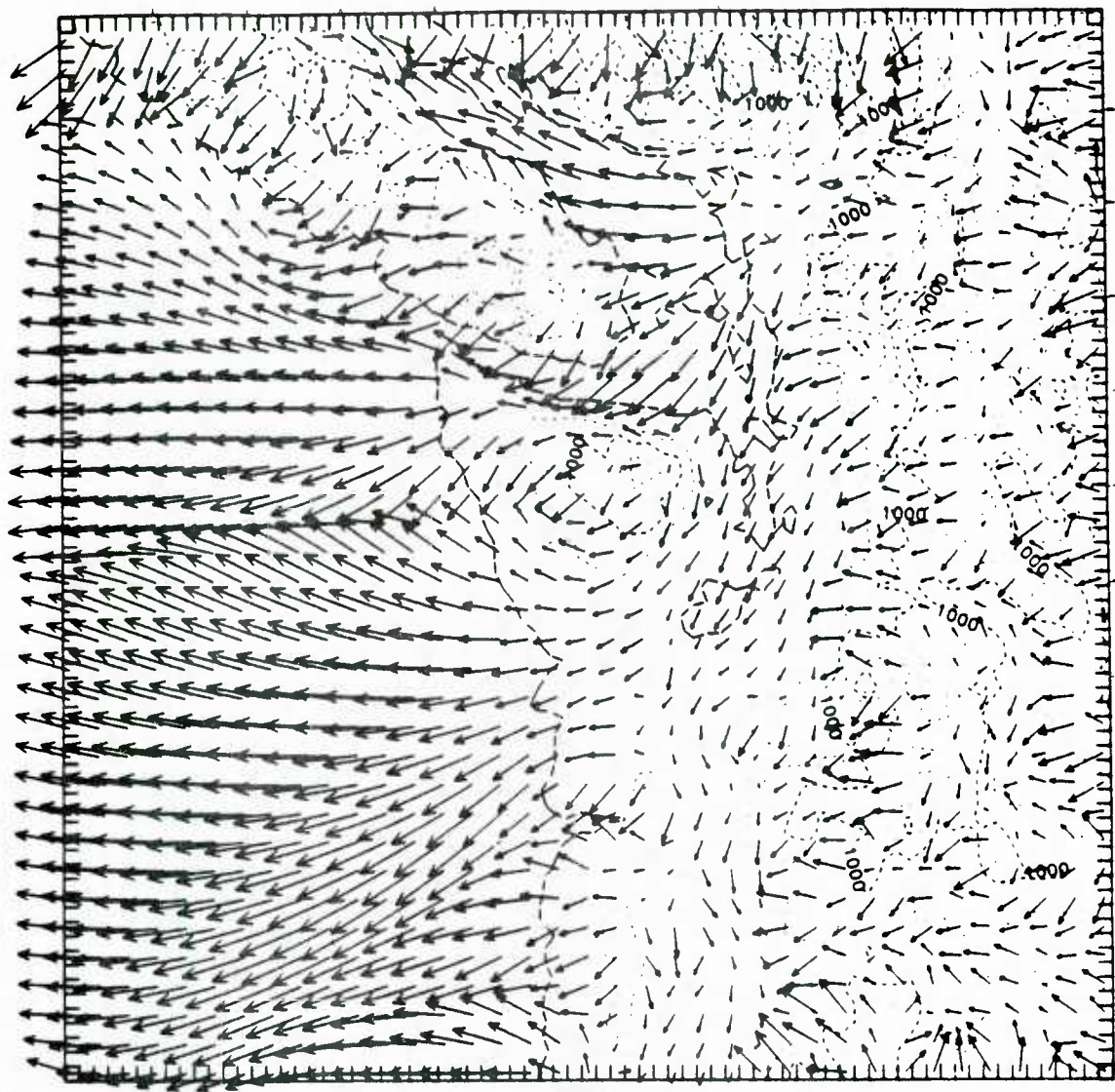
35

Figure 11d. Run for 23 November 1982, 12 GMT, observed surface winds.

Figure 11e. Run for 23 November 1982, 12 GMT, model surface
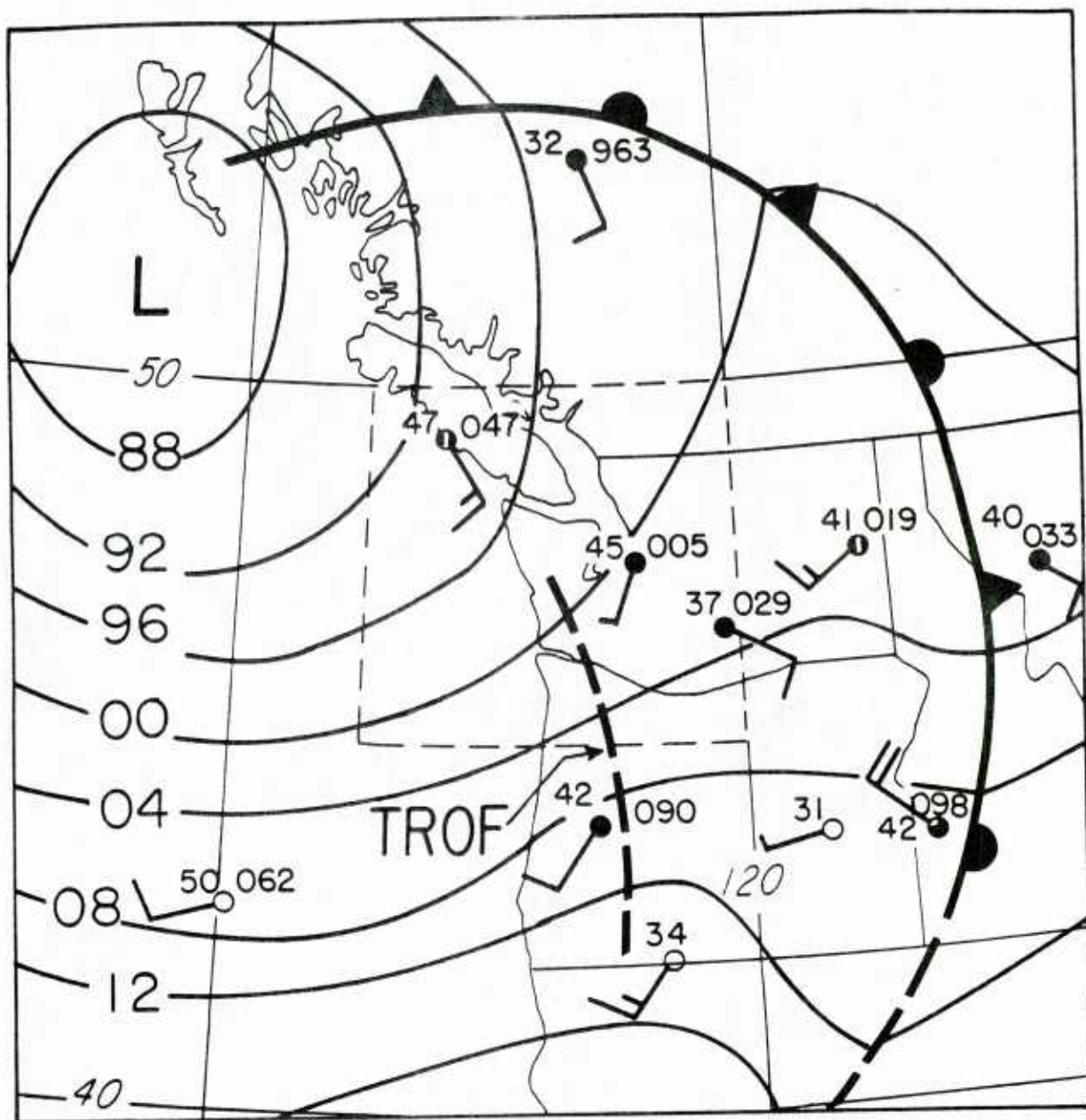winds with diabatic cooling.

37

Figure 12a. Run for 17 December 1982, 12 GMT, surface chart.

passed through the region during the previous 24 hours. The NMC analysis also indicates a weak trough in western Oregon and Washington at this time. The 850 mb flow, shown in Fig. 12b, clearly indicates a trough almost directly above the surface low, southwesterly geostrophic flow over western Washington State, and a ridge centered over western Alberta and northern Idaho. The upper air sounding at Salem, Oregon, the closest upstream station (Fig. 12c) indicates a nearly saturated adiabatic lapse rate through the lower troposphere and thus weak stability near the surface.

The observed surface mesoscale flow pattern (Fig. 12d) shows the winds on the coast turning from southwest to southeast as one moves northward up the coast. Winds over Puget Sound range from southerly in the south to southeasterly in the northern parts. This southeasterly flow continues up the Strait of Georgia. Probably the most interesting feature is what appears to be a cyclonic eddy north of the Olympic Mountains centered around a calm wind at Port Angeles on the south coast of the Strait of Juan de Fuca.

The model simulation of this situation, shown in Fig. 12e, included a cooling rate of 2.5°C per 6 h over land and .5°C per 6 h over water during the final 6 h of the run. As observed, winds over Puget Sound progress from southerly to south- southwesterly to southeasterly as one moves northwards. Winds in the Strait of Georgia are from the southeast with winds on the eastern shore north of Vancouver from nearly an easterly direction; this closely follows the actual pattern. Perhaps the most intriguing feature of the model wind field is the suggestion of the observed "eddy" north of the Olympic Mountains, although no calm winds are noted on the south side of the Strait of Juan de Fuca. Another interesting feature is the confluence line that parallels the coast.
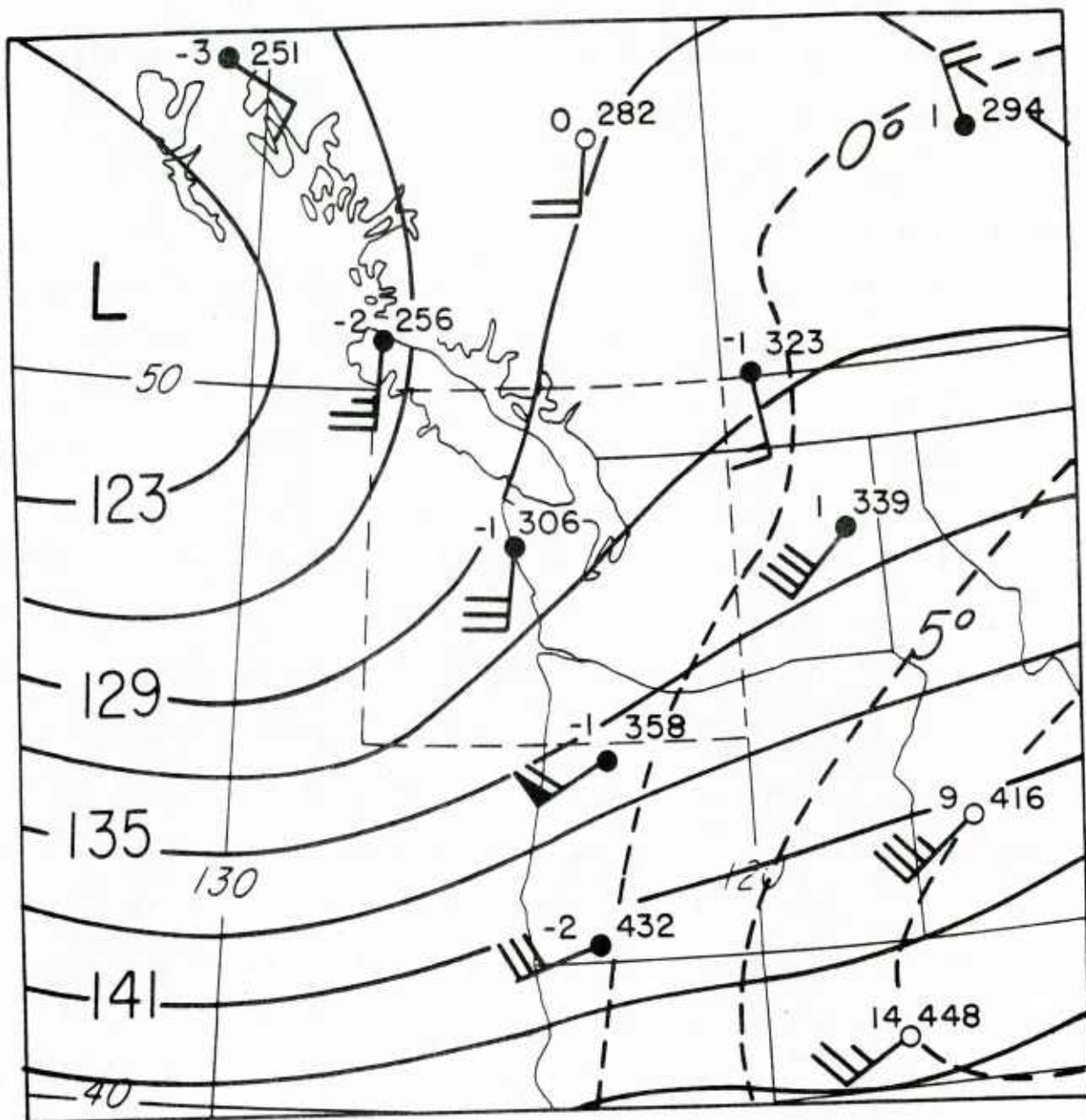
Figure 12b. Run for 17 December 1982, 12 GMT, 850 mb chart.
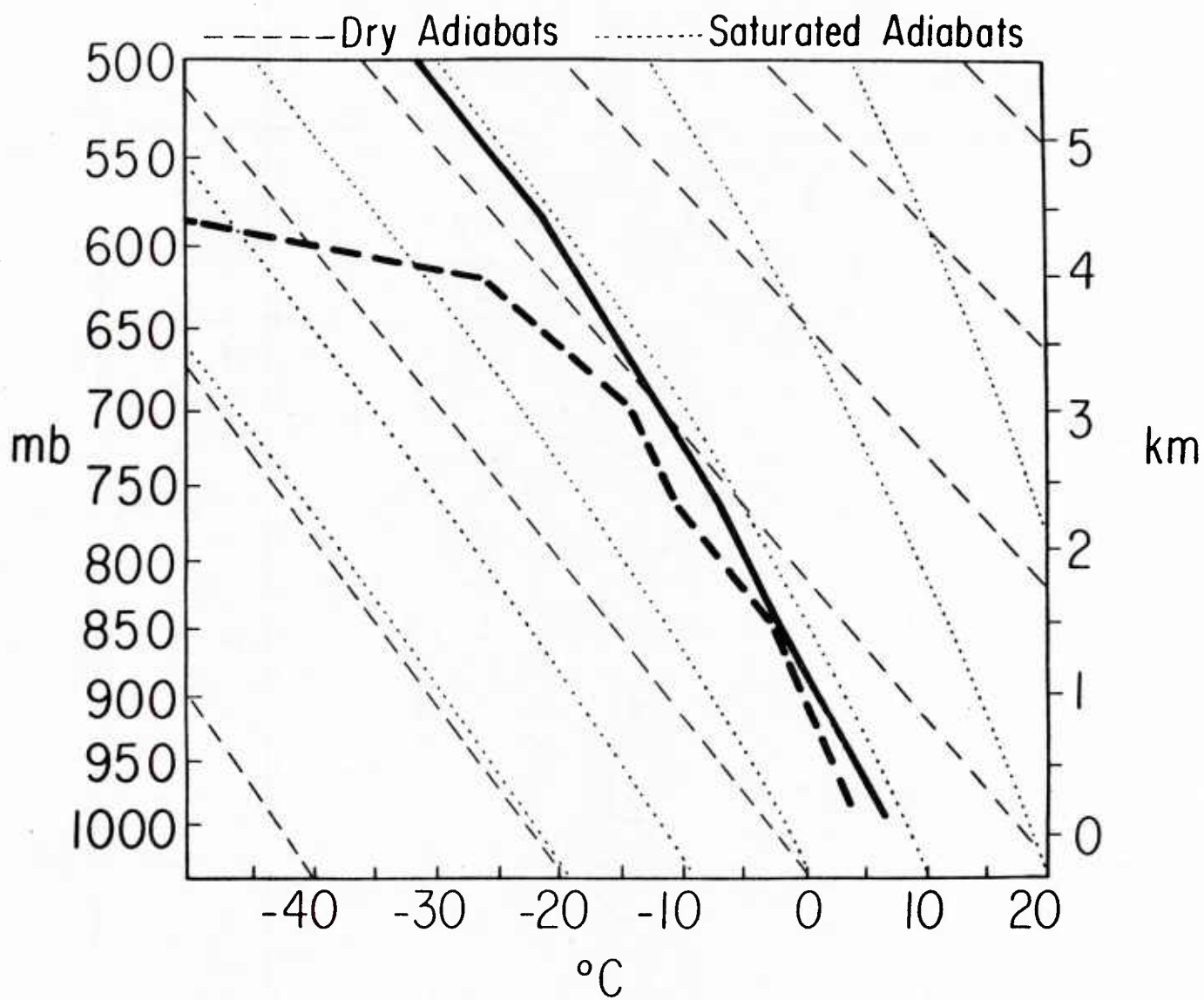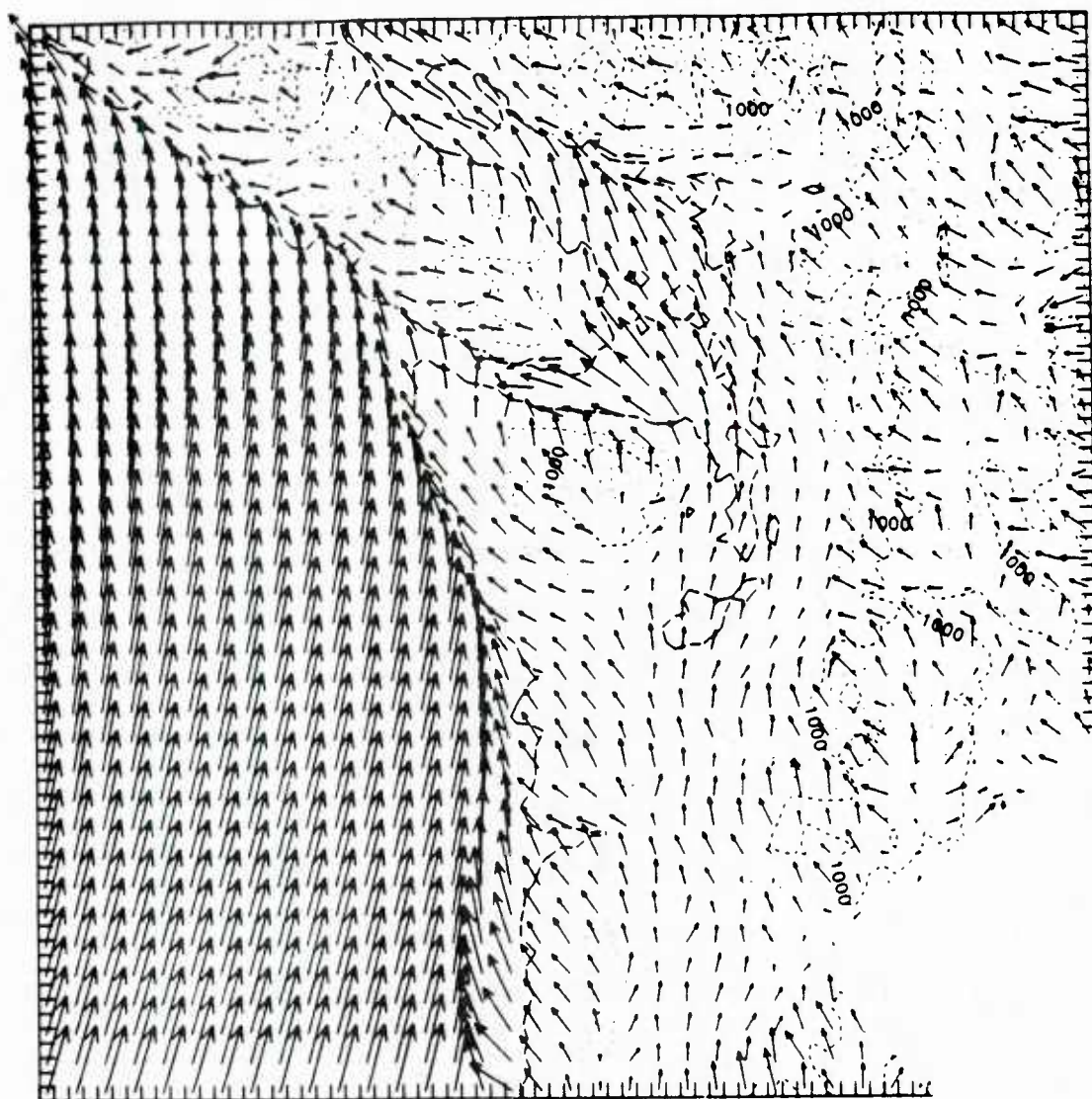
Figure 12c. Run for 17 December 1982, 12 GMT, sounding at Salem, OR.

Figure 12d. Run for 17 December 1982, 12 GMT, observed surface winds.

Figure 12e. Run for 17 December 1982, 12 GMT, model surface winds with diabatic cooling.

2. Mass Conservation Model

This model produced (as shown in Fig. 13) a quasi-uniform field of
southeasterlies with some minor deflection around the Olympic Mountains.
Certainly a poor simulation of the actual winds.

3. Mixed layer model blew up.

D. May 9, 1983 at 12 GMT: Westerly large scale surface flow with moderate
diabatic cooling.

At this time the large scale surface synoptic pattern (Fig. 14a) shows a
trough oriented southeast-northwest to the north of Washington State with lowest
pressures to the east. A ridge was building to the southwest. At 850 mb
(Fig. 14b) a similar pattern was observed. The sounding at Quillayute, Washington
at this time (Fig. 14c) indicates a shallow surface inversion, above which exists
a weakly stable layer to 850 mb. The observed mesoscale surface wind field is
shown in Fig. 14d. Along the coast there is a meeting between weak westerlies
from off the Pacific and weak easterlies, the latter being a drainage flow/land
breeze caused by nighttime cooling. Southerly flow moving up Puget Sound meets
a westerly flow near the eastern terminus of the Strait of Juan de Fuca. Also
note the calm winds in the western part of the Strait and the westerlies that
dominate much of the Strait of Georgia.

1. Mass-Dempsey Model.

The results of a model run with 3°C cooling over land and 1°C cooling over
water are shown in Fig. 14e. As in the observed windfield the Washington coast is
a meeting place between westerlies from off the Pacific and easterlies forced by
cooling over land. Before cooling was added to this simulation westerlies
completely dominated the coastal region. The model is able to duplicate the
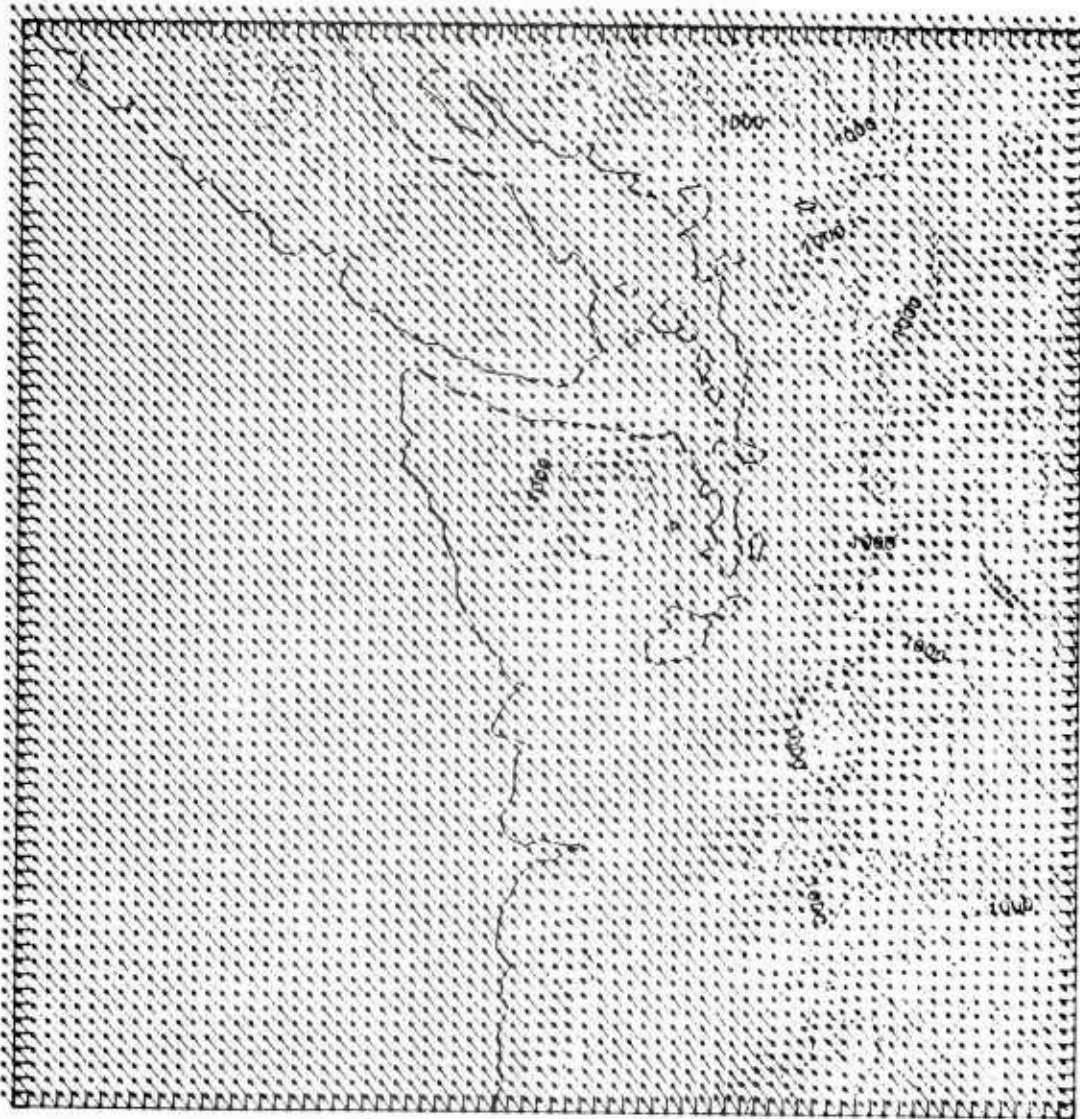
44

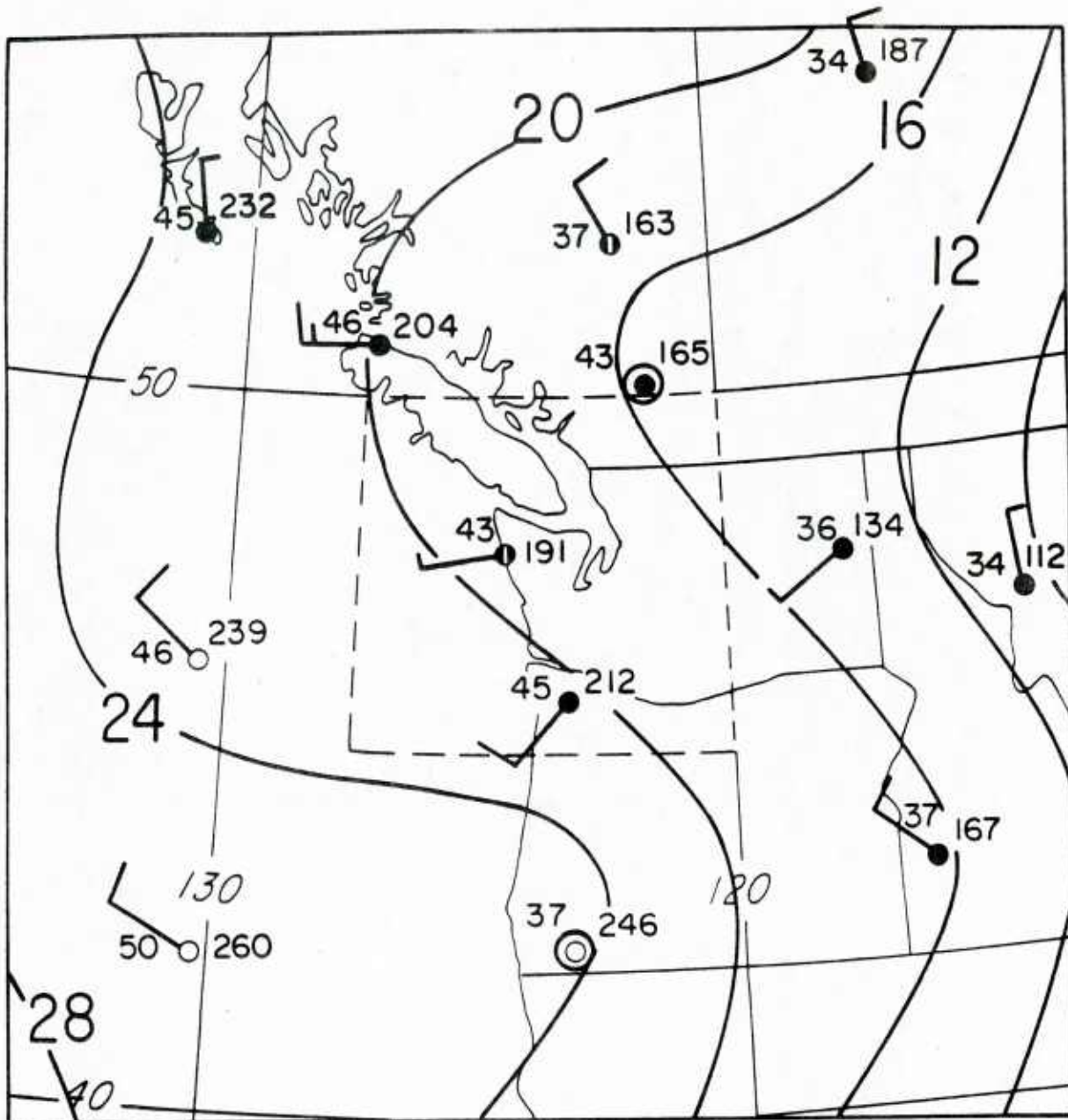Figure 13. Mass conservation model winds for Dec. 17, 1982.

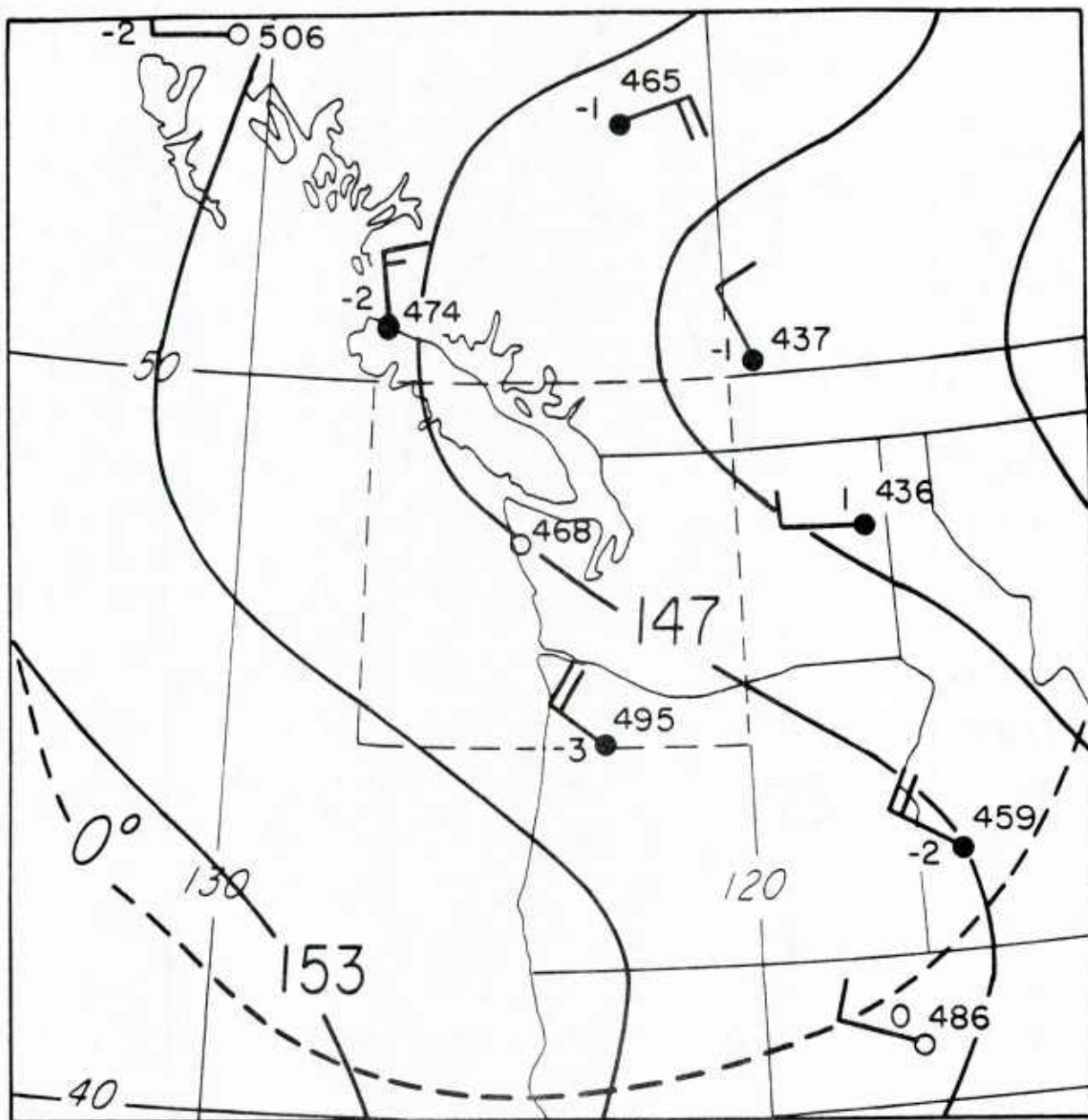Figure 14a. Run for 9 May 1983, 12 GMT, surface chart.

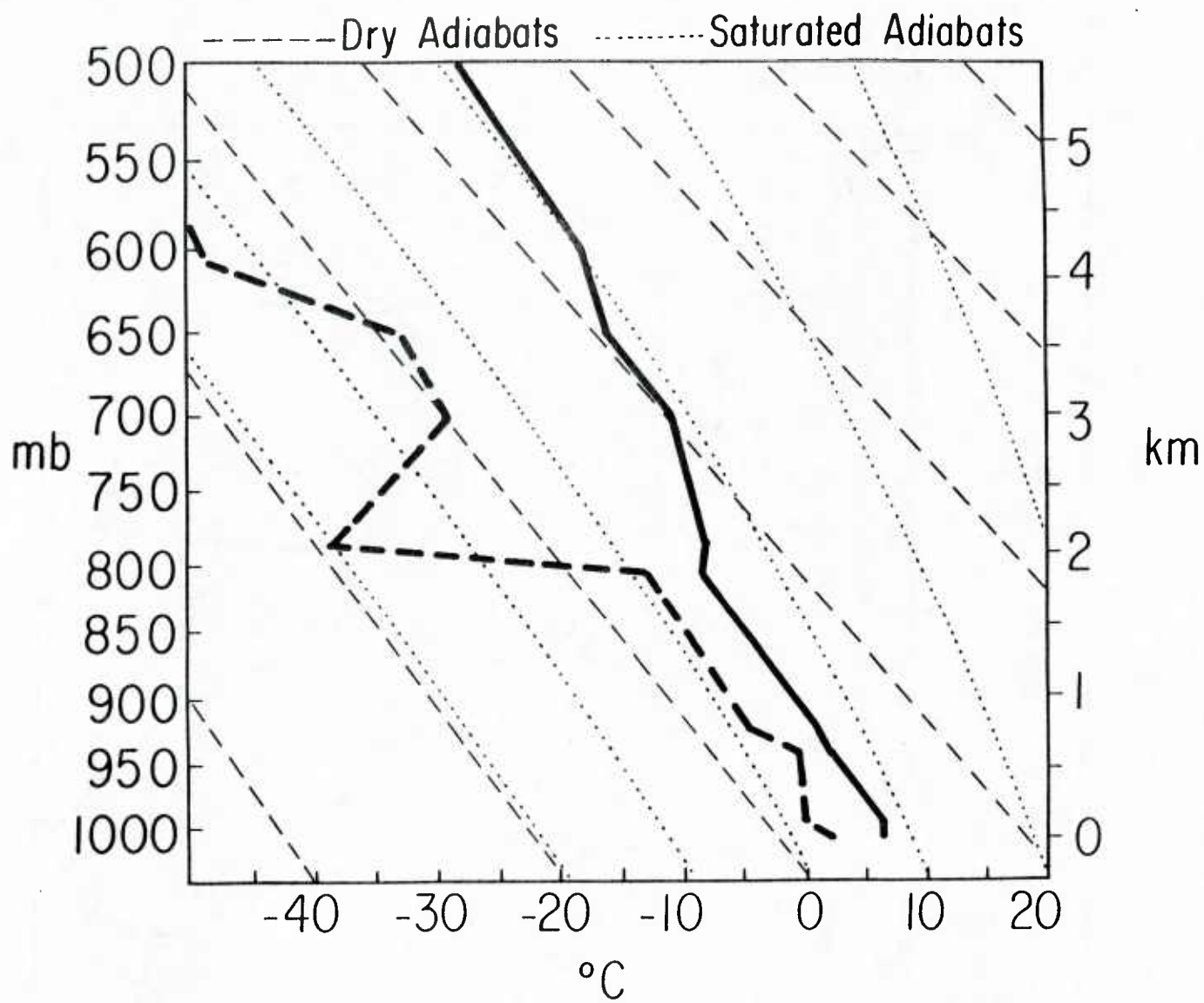Figure 14b. Run for 9 May 1983, 12 GMT, 850 mb chart.

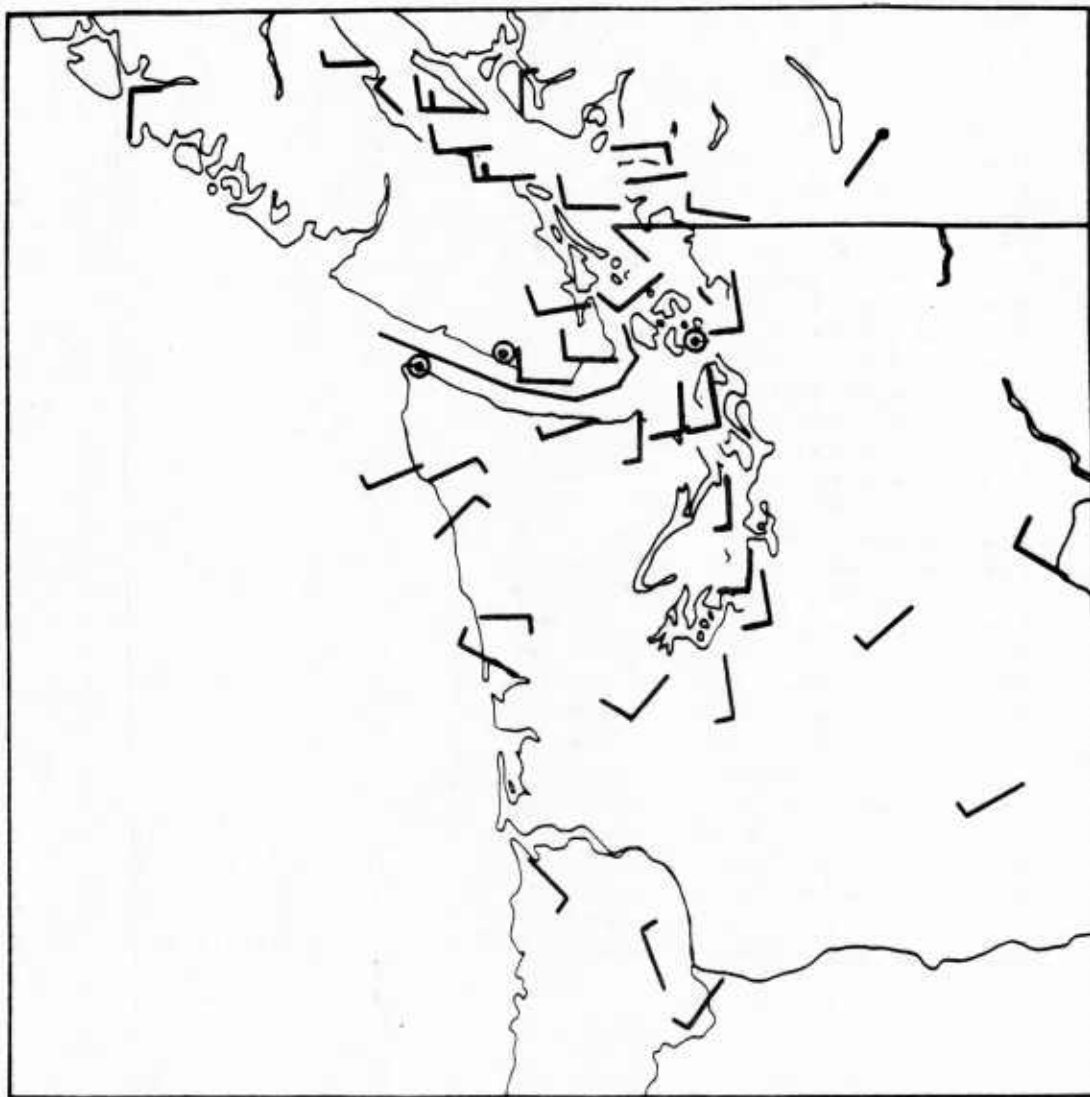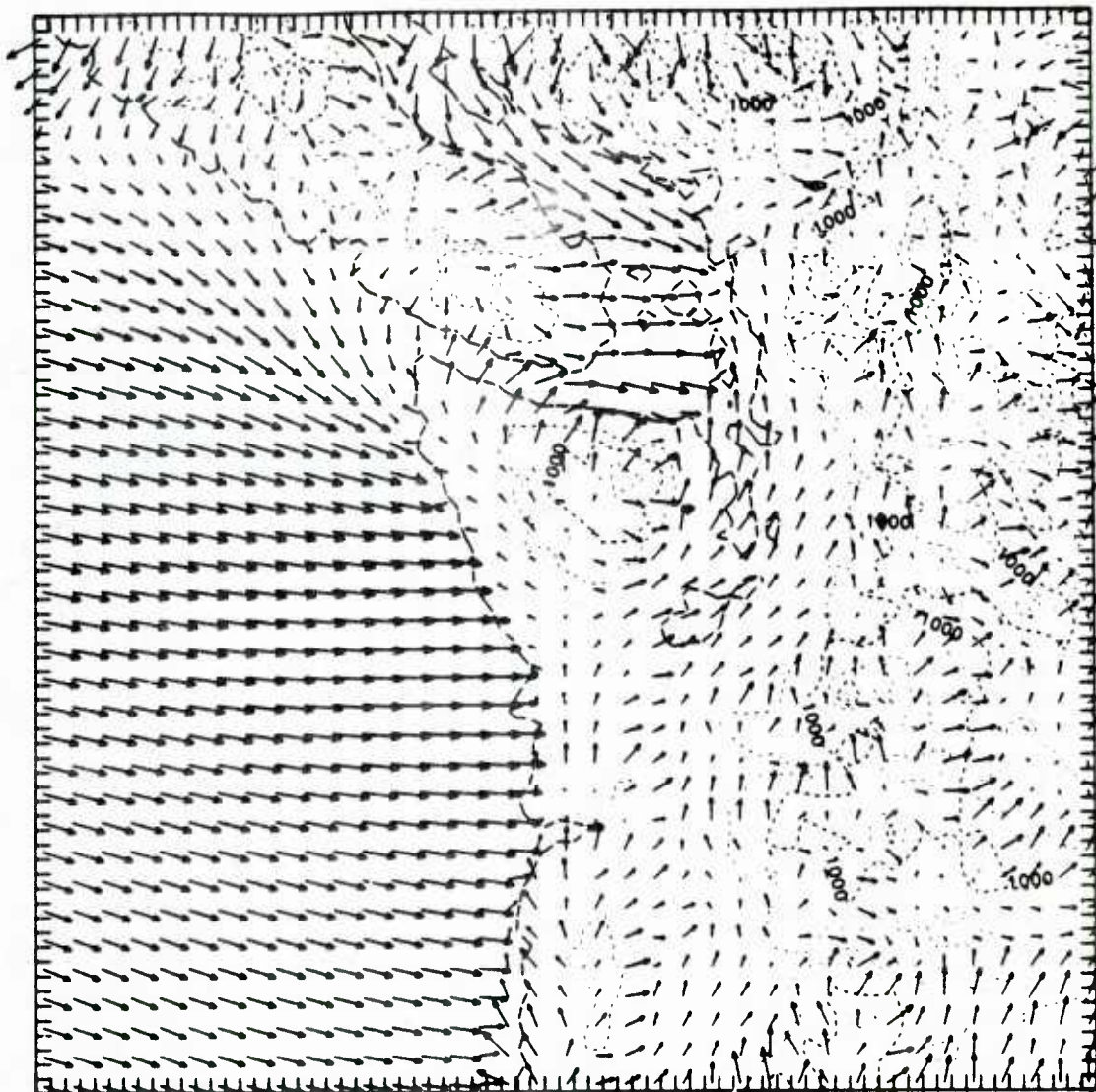Figure 14c. Run for 9 May 1983, 12 GMT, sounding at Quillayute, WA.

Figure 14d. Run for 9 May 1983, 12 GMT, observed surface winds.

Figure 14e. Run for 9 May 1983, 12 GMT, model surface winds with diabatic cooling.

observed southerlies in Puget Sound and the abrupt confluence with westerlies
east of the Strait of Juan de Fuca. At the western end of the Strait of Juan de
Fuca the model indicates calm winds in a region oriented southwest-northeast
across the western Strait of Juan de Fuca. This feature is amazingly similar to
the observed configuration. An apparent failing of the model is the excessive
northerlies in the northern Strait of Georgia, close to the model boundary.

2.   Mixed Layer Model

The results of a mixed layer run (without cooling) for May 9, 1983 is shown
in Fig. 15. Westerlies dominate the coast since no drainage flows off the
Olympics are occurring. Flow in Puget Sound is southeasterly, rather than the
observed southerly direction. Again, we note problems on the lateral boundaries.

3.   Mass Conservation Model

This run (shown in Fig. 16) possessed generally weak westerlies with some
speed-up over mountain crests. Surely a poor simulation.

b.   San Francisco Bay Cases

A.   March 23, 1983 at 00 GMT.

As shown in Fig. 17, at this time the surface winds indicated generally
westerly flow except for a southeasterly wind at MOD. The 850 mb chart at this
time (Fig. 18) shows a generally zonal flow over this region.

1.   Mass-Dempsey Model.

A model run (Fig. 19) with moderate heating (3°C per 6 hr) shows westerly
flow across San Francisco Bay which turns northeastward (somewhat excessive)
as it progresses inland. South of the Bay a current turns northwestward south
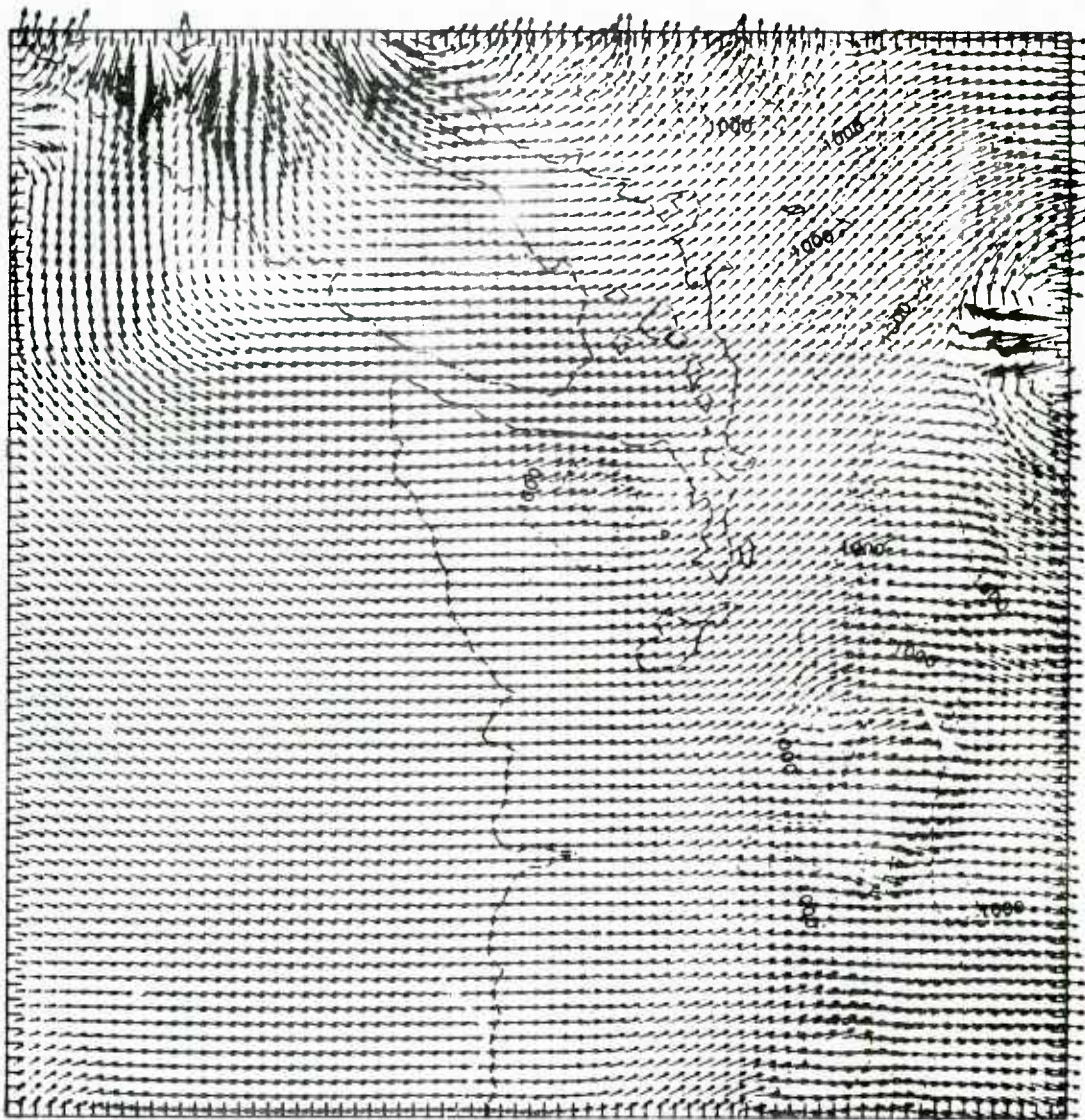of the location of MOD.

51

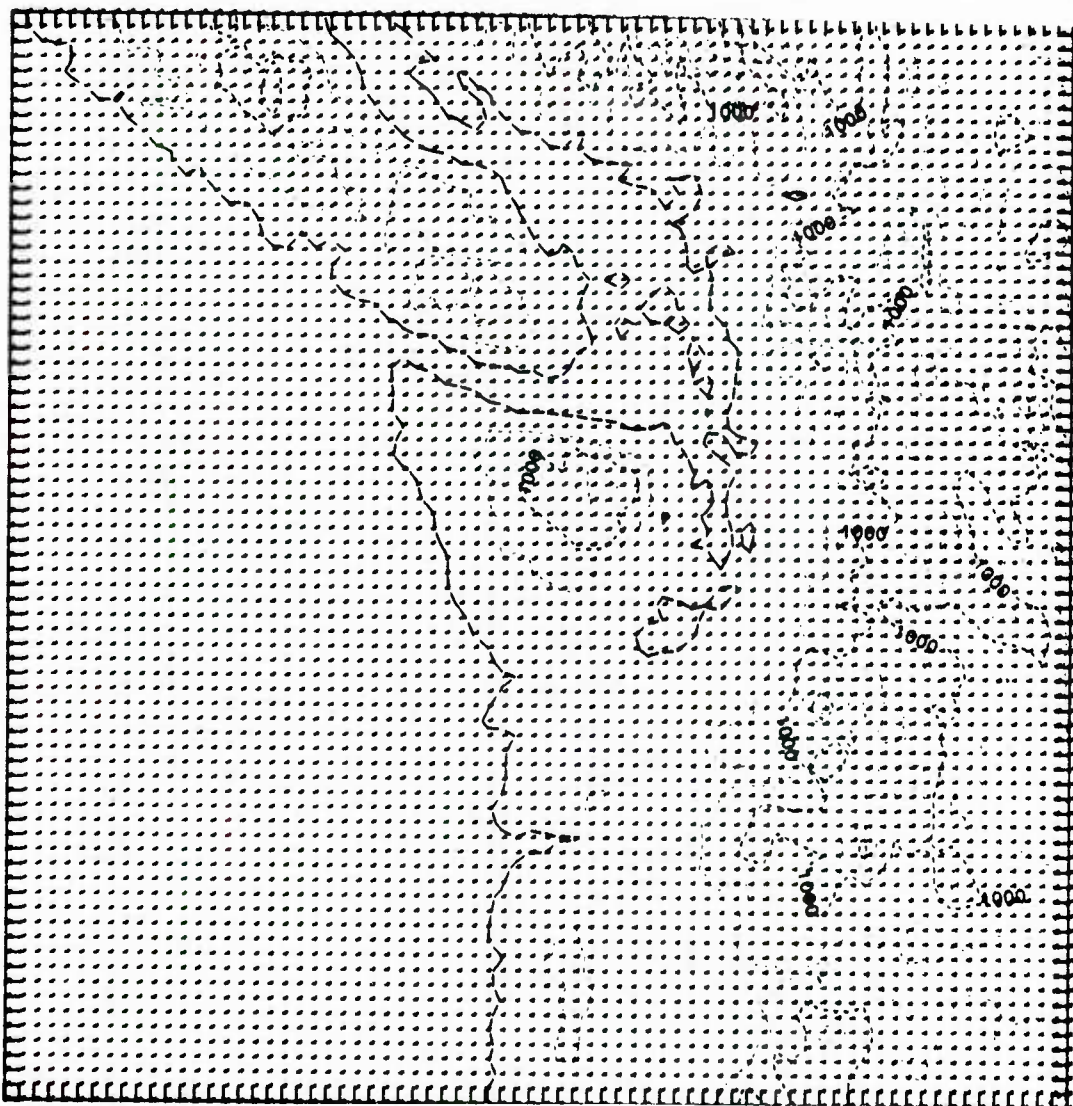Figure 15. Mixed layer model winds for May 9, 1983 at 12 GMT.

Figure 16.   Mass conservation model winds for May 9, 1983 at 12 GMT.
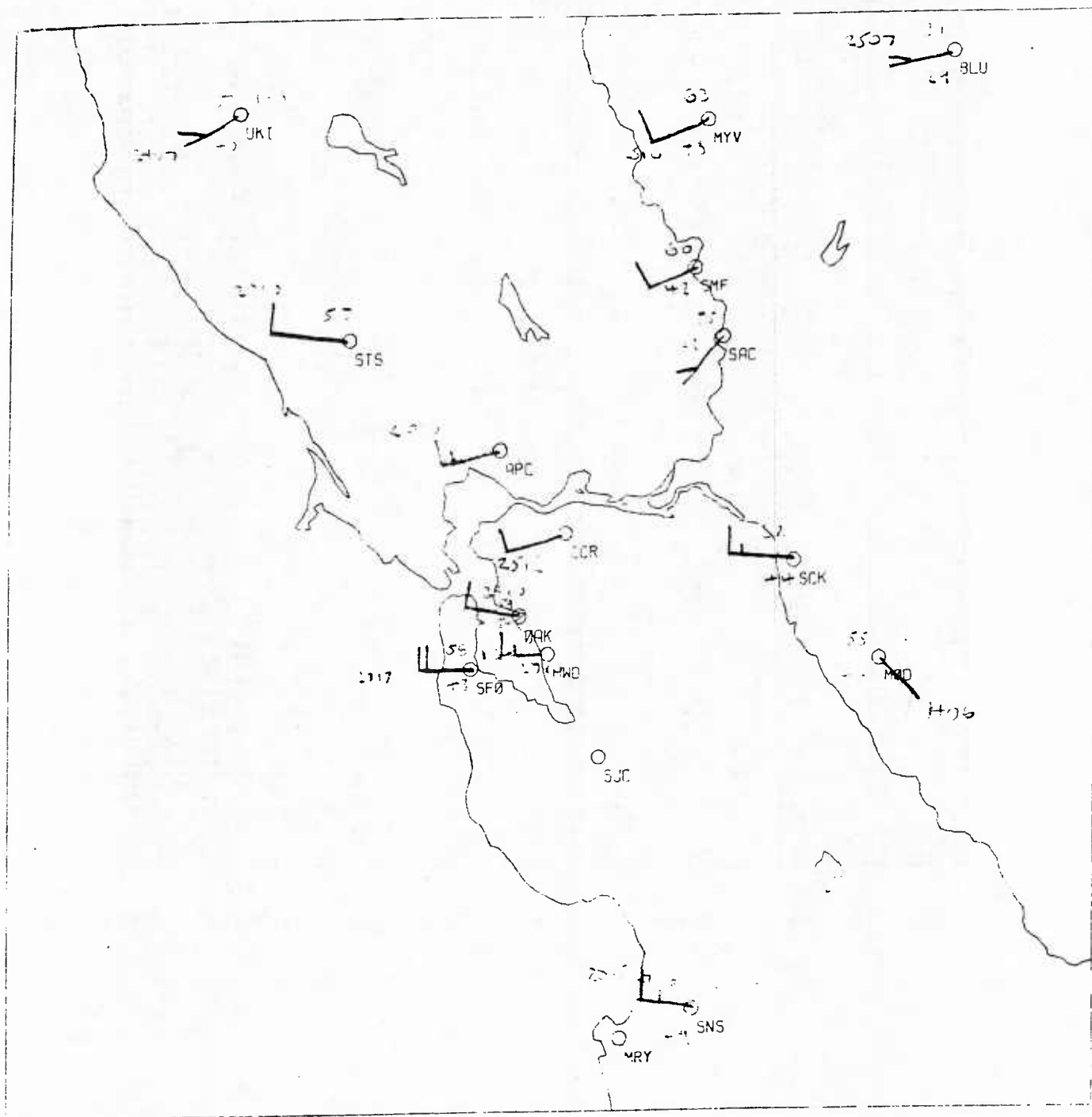
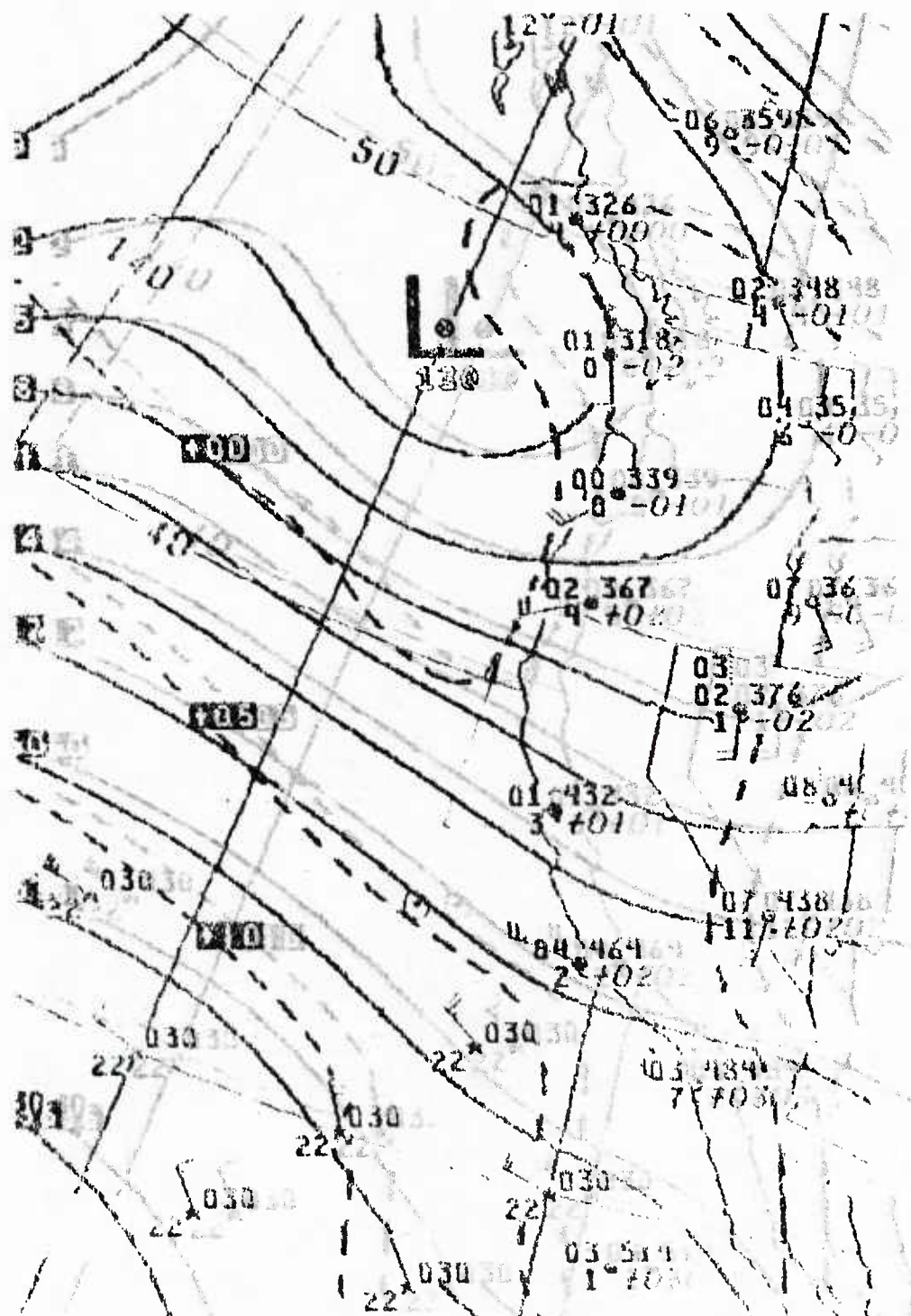Figure 17.   Surface observations for March 23, 1983 at 00 GMT run.

54

Figure 18. 850 mb height and temperature fields for March 23, 1983 at 00 GMT.
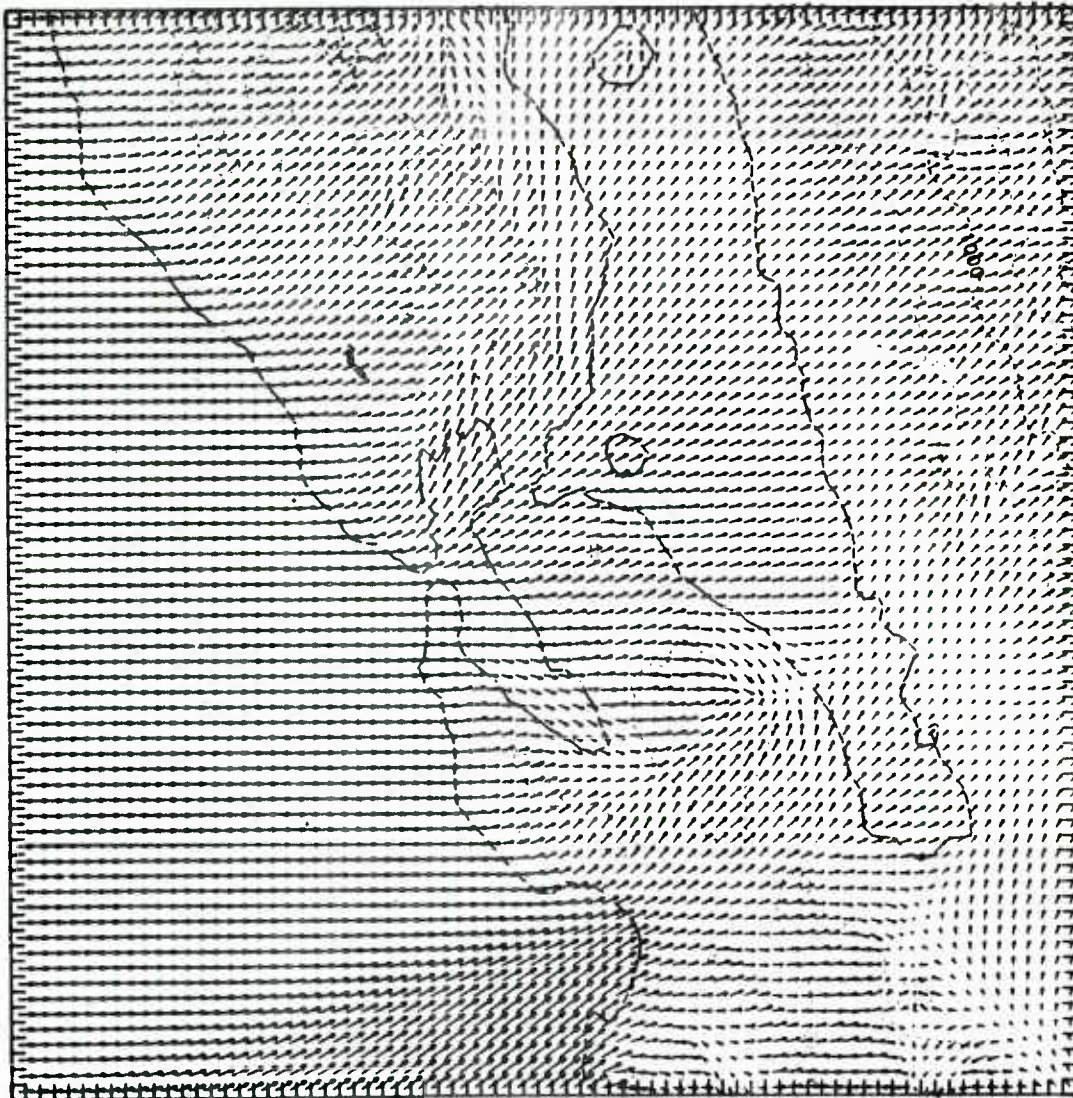
Figure 19.   Mass-Dempsey model surface winds for March 23, 1983.

2. Mixed Layer Model.

As indicated by the model wind field shown in Fig. 20 there were big problems so that little confidence could be put in these results.

3. Mass Conservation Model.

This run (Fig. 21) shows a northwesterly flow with only minor topographic deflection.

B. April 3, 1983 at 00 GMT

The surface wind field at this time (Fig. 22) shows moderate northwesterlies in coastal regions with some directional variation inland. The 850 mb chart (Fig. 23) indicate a weak southwest-northeast ridge in the Pacific Northwest with generally northerly flow over the central California Coast.

1. Mass-Dempsey Model.

A run of this model with moderate heating (5°C per 6 hr over land, 1°C per 6 hr over water) produced the wind field shown in Figure 24. As with the observed wind field, northwesterlies occur along the coast and in the Bay region with a turning towards the southeast in the southern inland basin (e.g., station MOD). In general, this run is quite good.

2. The Mixed Layer Model.

The model run (shown in Fig. 25) indicates northwesterly winds over much of the domain but could not duplicate the turning over the central Basin. Again, the boundaries are a real problem.

3. Mass Conservation Model.

As shown in Fig. 25, this model produced a nearly uniform west-northwesterly flow field with some minor channeling over crests.

57
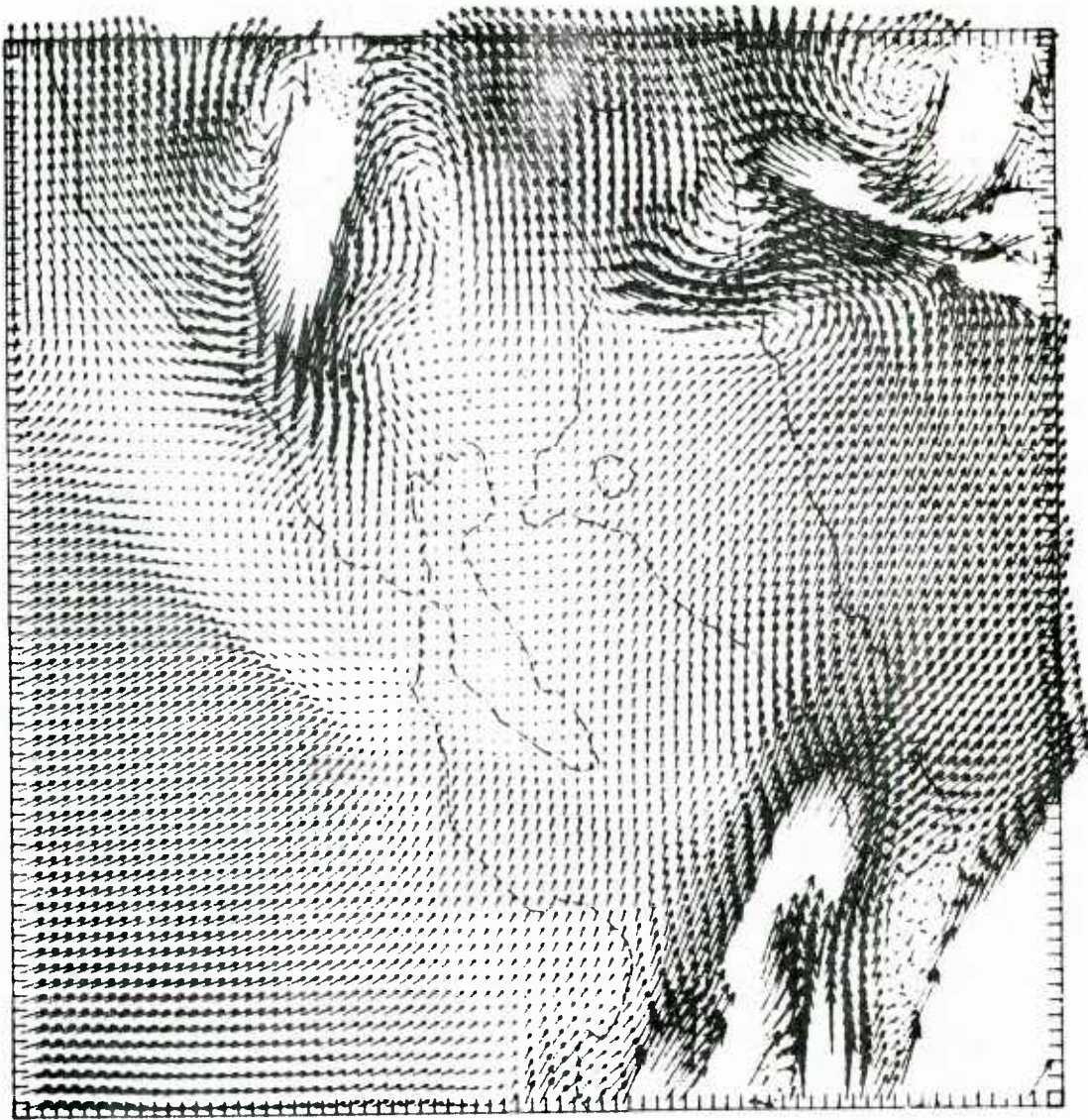
Figure 20. Mixed layer model surface winds for March 23, 1983 case.
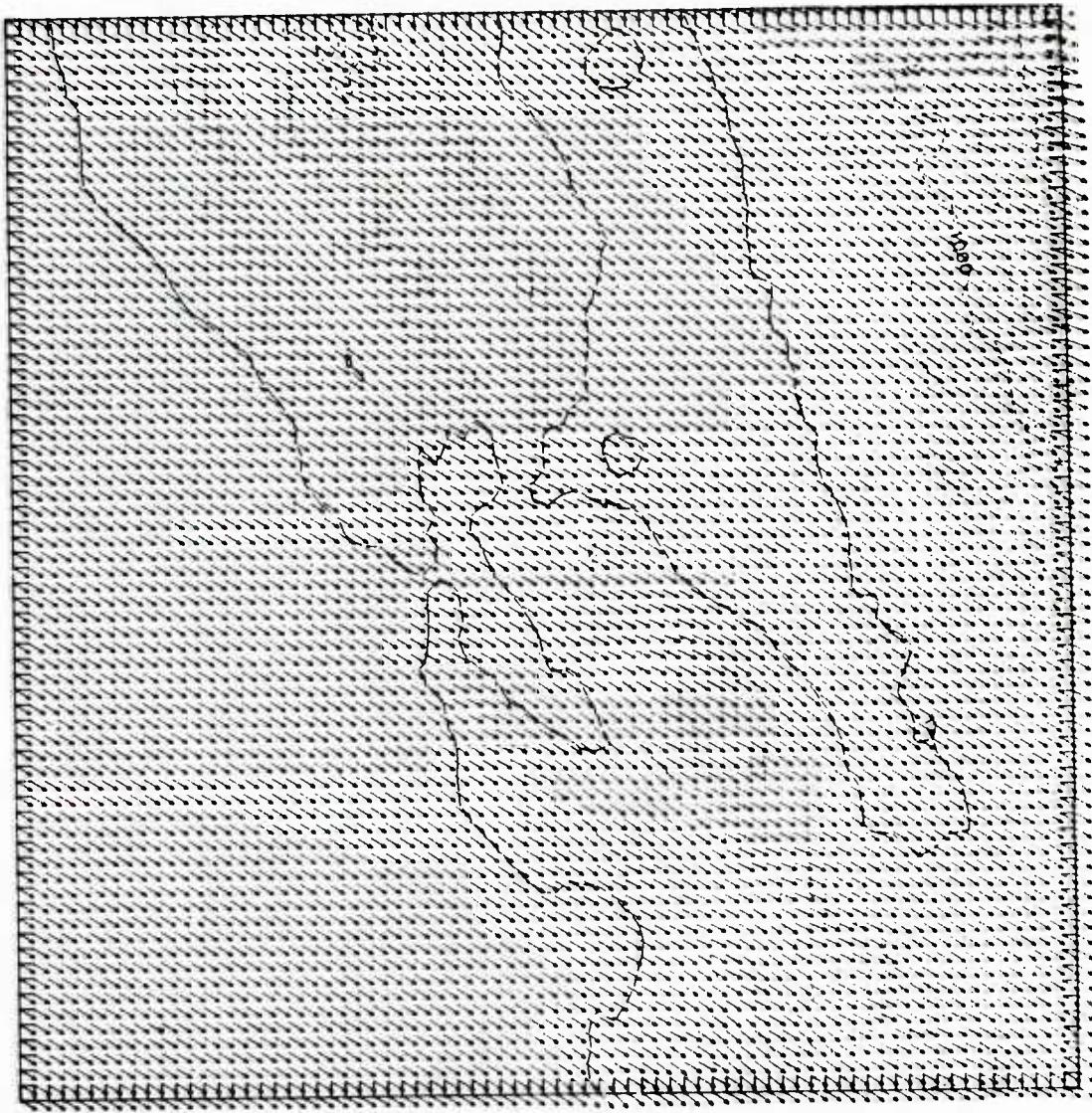
Figure 21. Mass conservation model surface winds for March 23, 1983 case.
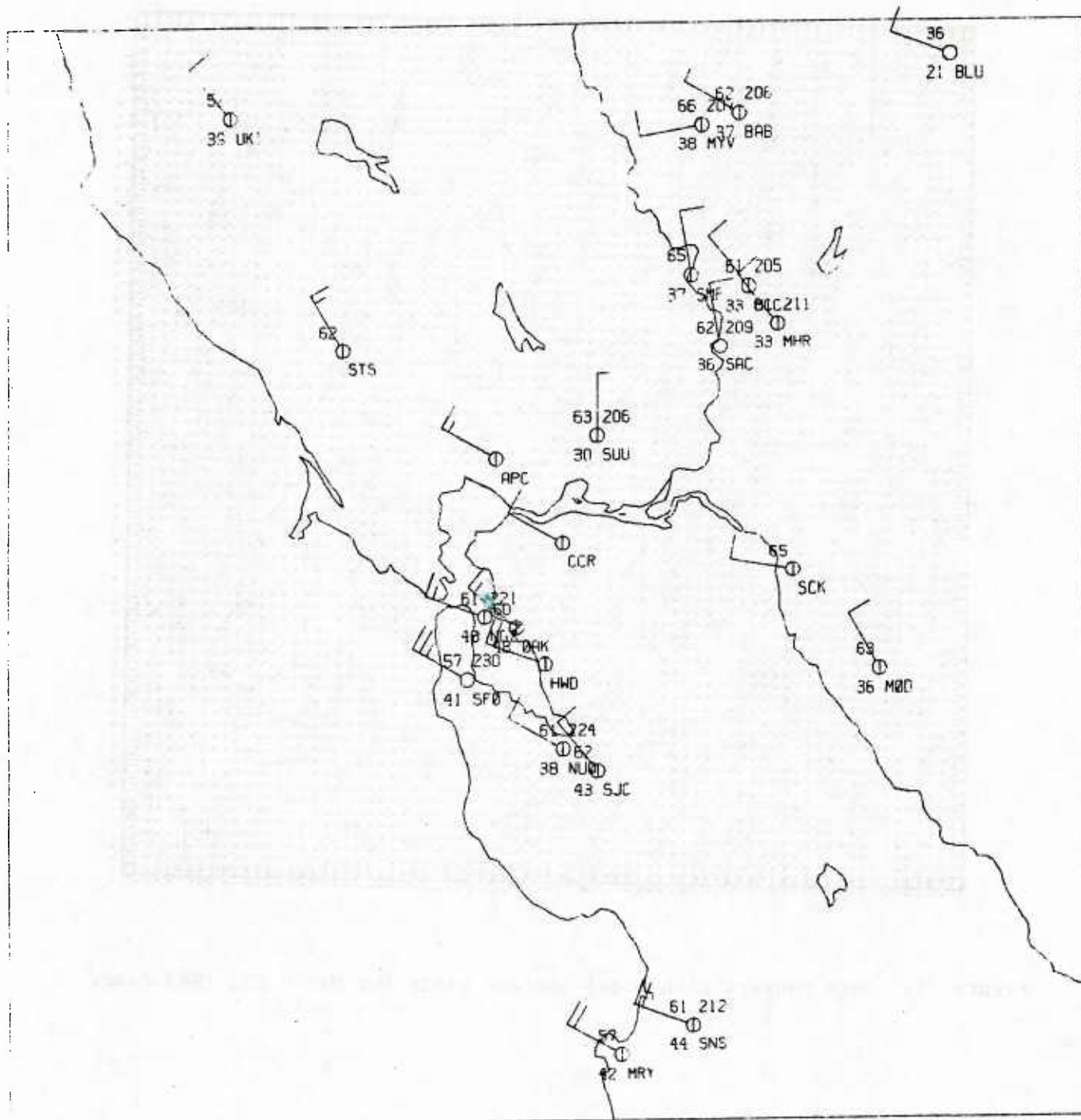
Figure 22.   Surface observations for April 3, 1983 at 00 GMT case.

Figure 23.   850 mb heights and temperature for April 3, 1983 at 00 GMT case.
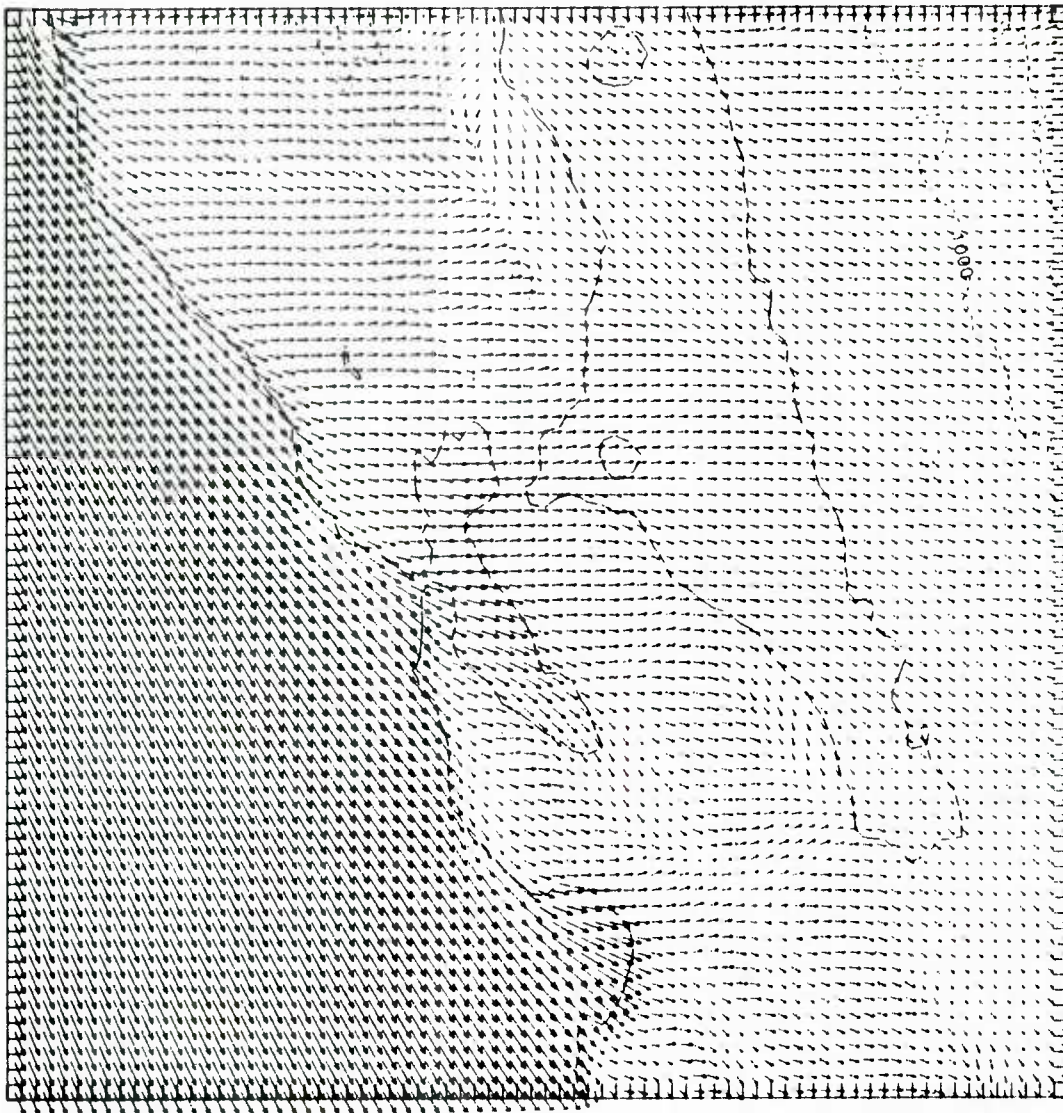
Figure 24. Mass-Dempsey model surface winds for April 3, 1983 at 00 GMT.

Figure 25. Mixed layer model winds for April 3, 1983 at 00 GMT case.
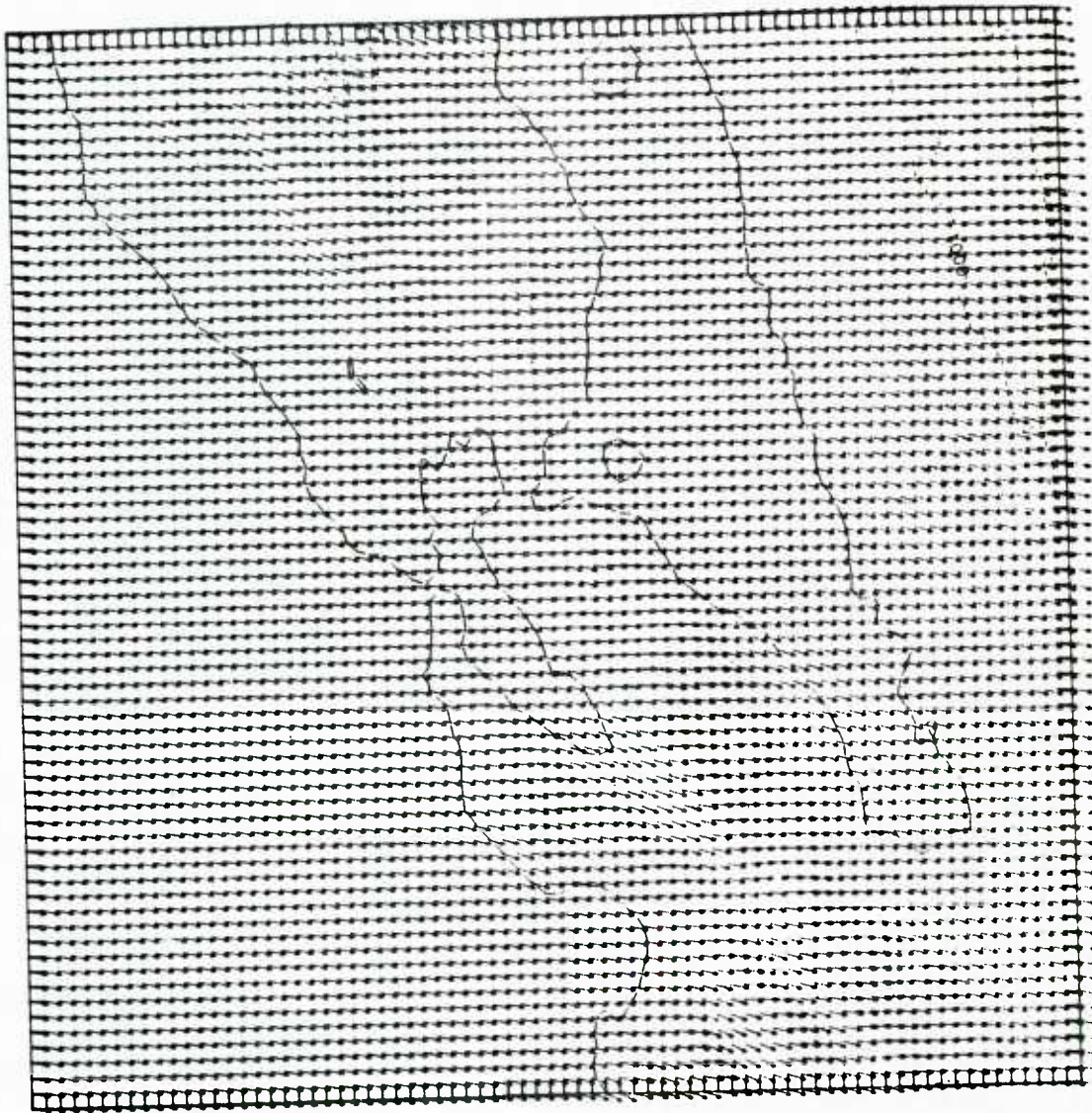
Figure 26. Mass conservation model winds for April 3, 1983 at 00 GMT case.

c. Subic Bay Case

In May 1976, Tropical Storm Olga swept close to Subic Bay and produced substantial damage to ships in the harbor of Port Olongapo. These model runs are an attempt to diagnose the wind field at May 24, 1976 at 0z near the height of the storm. The model topography shown in Figure 7 indicates that moderate topography surrounds the Subic Bay region. Wind during this time were generally southeasterly and thus the greatest damage occurred where the hurricane winds had the largest fetch. For this case the model was run at 2 km resolution.

1. Mass-Dempsey Model.

No diabatic forcing was included in this run. As shown in Figure 27, strong winds entered Subic Bay but were deflected in other areas by the surrounding topography.

2. Mixed Layer Model.

Went unstable due to the high wind speeds

3. Mass conservation model not run.

4. Conclusions and Summary

This report has shown the results of applying three relatively simple numerical models to the problem of diagnosing surface wind flow in complex terrain. Three test areas: the western Washington State, the San Francisco Bay Area and Subic Bay were used to test the three models: a one-level sigma coordinate model (Mass-Dempsey), a mixed layer model (Overland et al.) and a
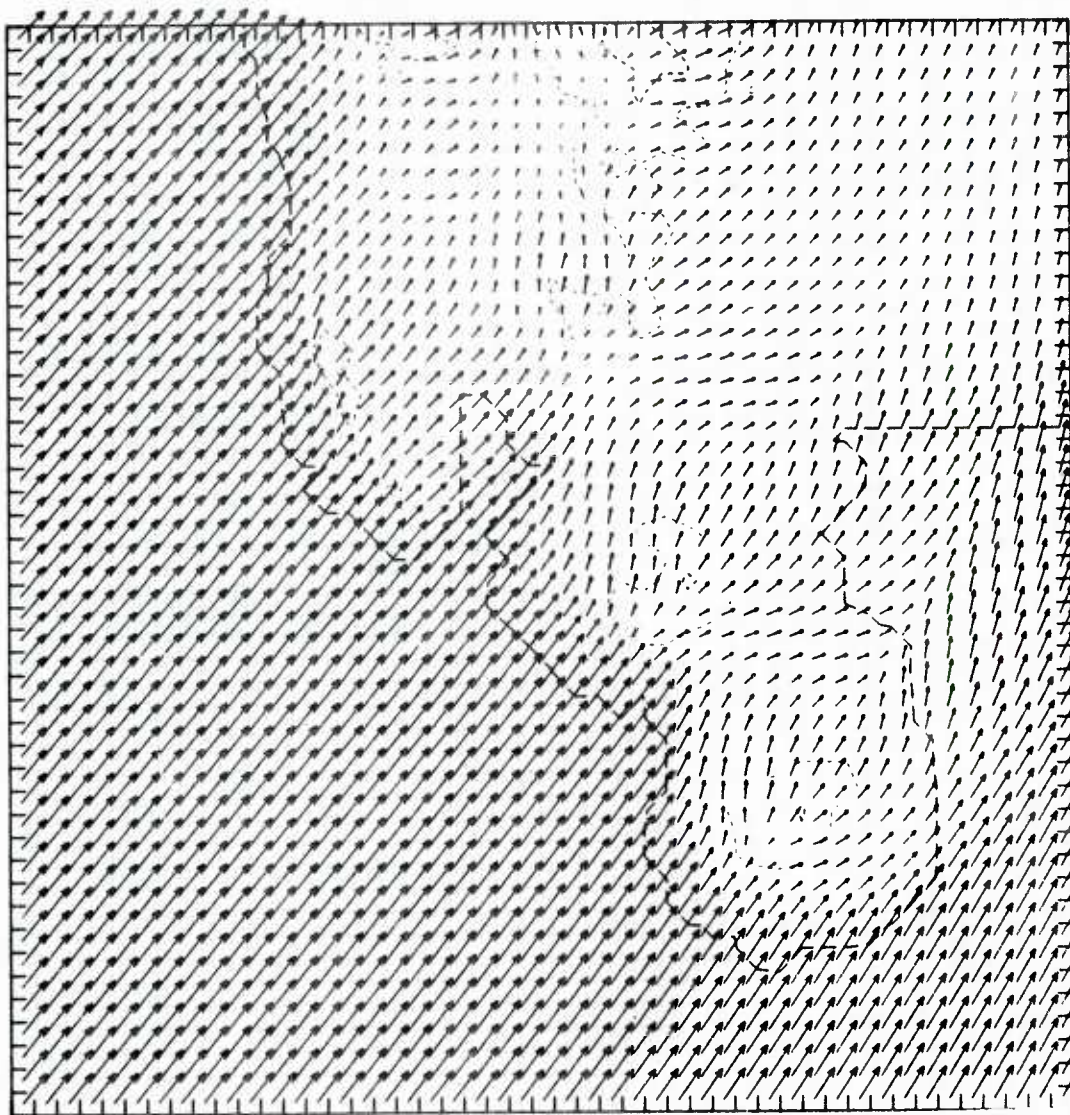
Figure 27. Mass–Dempsey model surface winds for May 24, 1976 at 00 GMT.

mass conservation model (Sherman). The results clearly indicate that the former model is generally superior for all three regions. Thus, it appears that the model[1] possesses much of the essential physics that determines flow in such regions. This fact may come as a surprise at first, considering the model's simplified physics, the lack of the continuity equation, the use of only one level, and the corresponding inability to model the effects of upper level changes forced by the topography.

Why does the model do so well? Even more basic is the question of how the flow in the model is deflected and blocked by higher terrain. To answer these questions first consider that the sigma coordinate geometry of the model imposes, a priori, a condition that there will be no flow through the surface. The surface flow in the model is deflected around, rather than over, higher terrain as a result of the adiabatic cooling and warming (third term in Eq. 4) experienced by stably stratified air as it rises and sinks over terrain features. For example, consider a model run with stably stratified flow initially moving directly towards an isolated range of mountains. At first the flow moves up and over the topography with little apparent deflection. However, as time progresses the upward motion on the windward side produces adiabatic cooling that results in an increase of surface pressure. Similarly, descending air on the leeward side produces warming and pressure falls. The flow responds to this asymmetric pressure pattern by being deflected around the windward slopes and then converging on the leeward side. A similar process will force air to flow parallel to the ridge line of a mesoscale valley. It should be noted that this adiabatic mechansim is the sole way by which modeled flow is forced to be channeled and deflected around higher terrain. The model's ability to duplicate most of the major mesoscale features in the cases cited above implies that this simple adiabatic

[1]All further use of "the model" refers to the Mass-Dempsey model.

On a 74 by 75 point grid with a horizontal resolution of approximately 7.5 km the Mass-Dempsey model took about 66 seconds on the CRAY 1 at NCAR. About a third of this was fancy graphics and diagnostics that would not be required for operational use. Thus, let us assume a time of 44 seconds. From benchmarks between the PRIME 400 and the CRAY 1 we know that the model run would take about 367 minutes or 6 hours on the PRIME 400. From the information I have gotten from HP, the 9845 is about twice as fast as the IBM XT. From several PRIME 400/IBM XT benchmarks we have found a speed rate of 26. Thus, the IBM 9845 should be 13 times slower than the PRIME 400 or 78 hrs (3.25 days). Clearly, the model is too slow to run even quasi-operationally on the 9845 even cutting back on the array size by half. What about the Eclipse S/250? From a single benchmark it appears that the PRIME 400 and Eclipse S/250 are roughly equivalent in speed. Thus, a 6 hr. run time would be expected using the above 74 x 75 grid. However, by reducing the grid and using a less conservative steady state criterion, the model runs could probably be reduced to 1 - 3 hrs. This is still somewhat long for an operational run but possible.

It should be noted that memory capacity is not a problem on either the HP9845 or Eclipse S 250.

Another way of handling the problem would be to run a large series of model runs for various synoptic directions and vertical stabilities for each domain of interest to the Navy and to put them into an operational manual. These model runs could be done on a main frame and this run time would not be significant.

Finally, it is important to note that the Mass-Dempsey model requires very limited data for initialization and thus is quite appropriate for data poor regions. The mass conservation and mixed layer models also require relatively modest initial data; however, they do require mixed or boundary layer heights which are often difficult to accurately determine.

REFERENCES

Anderson, G. E., 1971: Mesoscale influences on wind fields. J. Appl.
Meteor., 10, 377-386.

Anthes, R. A., and T. T. Warner, 1978: Development of hydrodynamic models
suitable for air pollution and other mesometeorological studies.
Mon. Wea. Rev., 106, 1045-1078.

Cressman, G. P., 1959: An operative objective analysis scheme.
Mon. Wea. Rev., 87, 367-374.

Danard, M., 1971: Numerical study of the effects of longwave radiation and
surface friction on cyclone development. Mon. Wea. Rev., 99, 831-839.

Danard, M., 1977: A simple model for mesoscale effects of topography on
surface winds. Mon. Wea. Rev., 105, 572-580.

Dickerson, M. H., 1978: MASCON - A mass consistent atmospheric flux
model for regions of complex terrain. J. Appl. Meteor., 17, 241-253.

Fosberg, M. A., W. E. Marlatt, and L. Krupnak, 1976: Estimating airflow
patterns over complex terrain. USDA Forest Service research paper
RM-162, Rocky Mountain Forest and Range Experimental Station, Ft.
Collins, CO.

Gerrity, J. P.; R. D. McPherson and P. D. Polger, 1972: On the efficient
reduction of truncation error in numerical prediction models. Mon. Wea.
Rev., 100, 637-643.

Keyser, D., and R. A. Anthes, 1977: The applicability of a mixed-layer model
of the planetary boundary layer to real-data forecasting. Mon. Wea.
Rev., 105, 1351-1371.

Lavoie, R. L., 1972: A mesoscale model of lake-effect storms. J. Atmos. Sci.,
29, 1025-1040.

Lavoie, R. L., 1974: A numerical model of the trade wind weather on Oahu.
Mon. Wea. Rev., 102, 630-637.

Marwitz, J. D., 1983: The kinematics of orographic airflow during Sierra
storms. J. Atmos. Sci., 40, 1218-1227.

Mass, C., 1981. Topographically forced convergence in western Washington State.
Mon. Wea. Rev., 109, 1335-1347.

Mass, C., 1981: A single-level numerical model suitable for complex terrain.
Proceedings of the Fifth Conference on Numerical Weather Prediction,
American Meteorological Society, Boston, MA 02108, 316-319.

Mass, C., 1982: The topographically forced diurnal circulations of western
Washington State and their influence on precipitation. Mon. Wea. Rev.,
110, 170-183.

Mesinger, F., and A. Arakawa, 1976: Numerical methods used in atmospheric
models, Vol. I. GARP Publications Series No. 17.

Nickerson, E. C. and E. L. Magaziner, 1976: A three-dimensional simulation of
winds and non-precipitating orographic clouds over Hawaii. NOAA Technical
Report ERL 377-APCL 39.

Overland, J. E., M. H. Hitchman and Y. J. Han, 1979: A regional surface wind
model for mountainous coastal areas. NOAA Technical Report, ERL 407-
PMEL 32.

Overland, J. E. and B. E. Walter, 1981: Gap winds in the Strait of Juan de
Fuca. Mon. Wea. Rev., 109, 2221-2233.

Pielke, R., 1974: A comparison of three-dimensional and two-dimensional
numerical predictions of sea breezes. J. Atmos. Sci., 31, 1577-1585.

Reed, R. J., 1980: Destructive winds caused by an orographically induced mesoscale cyclone. Bull. Amer. Meteor. Soc., 61, 1346-1355.

Reed, R. J., 1981: A case study of a bora-like windstorm in western Washington. Mon. Wea. Rev., 109, 2384-2393.

Sherman, C. A., 1978: A mass-consistent model for wind fields over complex terrain. J. Appl. Meteor., 17, 312-319.

Staley, D. O., 1957: The low-level sea breeze of northwest Washington, J. of Meteor., 14, 458-470.

Walter, B. A. and J. E. Overland, 1982: Response of stratified flow in the ice of the Olympic Mountains. Mon. Wea. Rev., 110, 1458-1473.

Appendix I

Parameterization of Surface Friction

The frictional force in the boundary layer ($\vec{F}$) can be expressed as the vertical divergence of the shearing stress:

$$\vec{F} = -\frac{1}{\rho} \frac{\partial \vec{S}}{\partial Z} \qquad\qquad 1.1$$

where ρ is density and $\vec{S}$ is the shearing stress. At the surface the stress can be parameterized by a drag law

$$\vec{S}_s = \rho C_D \vec{V}_s |\vec{V}_s| \qquad\qquad 1.2$$

where C_D is a drag coefficient and $\vec{V}_s$ is the surface wind vector; above the boundary layer $\vec{S}$ can be considered to be negligible. If one assumes a linear stress profile that vanishes at the top of the boundary layer (or in our case at H, the top of the layer of topographic influence) the mean frictional force in the boundary layer can be estimated as:

$$\vec{F} = -\frac{1}{\rho} \left(\frac{\vec{S}_H - \vec{S}_s}{H} \right) = -\frac{C_D \vec{V}_s |\vec{V}_s|}{H} \qquad\qquad 1.3$$

Deardorff (1972) suggests that under neutral or stable conditions the stress vanishes at a height lower than the inversion or boundary layer height and accordingly the stress should be increased by a factor c of 2.8. In addition, because the stress profile under stable and neutral conditions is not linear but is more steeply sloped near the surface, the stress divergence at the surface (i.e., at 10 m in our case) is greater than the mean stress divergence for the layer as a whole (by approximately a factor of two in Deardorff, 1972). Furthermore, frictional boundary layers are typically lower (e.g. 1 km) than the layer of topographic influence hypothesized in our model

(2 km). For these reasons, we suggest that the surface frictional

force is about 4 times the estimate given in (3), so that

$$\vec{F}_s = - 4c\frac{C_D \vec{V}_s |\vec{V}_s|}{H} \qquad\qquad 1.4$$

where $\vec{F}_s$, the surface frictional force, is assumed to be directed

in the opposite direction of the surface wind. In our model we used

values of C_D of 2×10^{-2} over land and 1.4×10^{-3} over water. At each

model grid point we determined the percentage of water and land in the

surrounding 7.5 km square and scaled the drag coefficient

proportionately. This land/water percentage was also used in the

diabatic heating parameterization.

76

Appendix II

The Horizontal Diffusion Terms

The momentum (1) and thermodynamic energy (4) equations of this model possess horizontal diffusion terms to control computational instability and to represent the effects of horizontal subgrid-scale mixing. The momentum diffusion term is of the form $K_m \nabla_\sigma^2 \vec{V}_s$, where K_m is the momentum diffusion coefficient and the Laplacian ∇_σ^2, taken at the surface or $\sigma = 1$ level, is finite differenced using the method described in Danard (1971).

The temperature diffusion term in the thermodynamic energy equation (4) is of the form $K_T \nabla_H^2 T$, where K_T is the temperature diffusion coefficient and the Laplacian ∇_H^2 is taken on a horizontal plane rather than along the surface. To understand why a different Laplacian is used for this term, consider a hypothetical situation in which in which there are no large scale pressure (or height) or temperature gradients, no diabatic forcing, and a constant lapse rate everywhere. In such a case no surface flow should be produced by the model. However, if the temperature diffusion term uses a Laplacian evaluated at the surface, the Laplacian will generally be non-zero since surface temperatures usually vary non-linearly along slopes. The result is a non-zero diffusion term that forces spurious winds in the absence of large scale or diabatic forcing. Evaluating the Laplacian on a horizontal plane eliminates this problem. The finite difference form of this Laplacian is evaluated at the level of the center point with the temperatures at the surrounding points being vertically

extrapolated from the surface using the known local lapse rates.

The runs presented in this paper used diffusion coefficients (K_m and K_T) of either 2.5 or 3×10^4 m^2 s^{-1}.

Model Initialization

To begin an integration the model requires a lapse rate representative of the lower free atmosphere as well as the geopotential height and temperature fields at an undisturbed pressure level, in our case 850 mb. The lower tropospheric lapse rate is taken from the radiosonde sounding nearest the large scale inflow into the domain. The 850 mb heights and temperatures at each grid point are found by first subjectively interpolating the fields analyzed on the appropriate National Meteorologial Center (NMC) operational 850 mb chart to a 4 by 4 grid covering the model domain. Then an iterative Cressman (1959) scheme is used to calculate interpolated values on the model grid.

The initial surface temperature field is calculated by using the given lower tropospheric lapse rate and 850 mb fields:

$$T_s = T_{850} + \gamma (Z_{850} - Z_s) \qquad 3.1$$

where Z_s and Z_{850} are the heights of the surface and 850 mb levels at a point and γ is the lower tropospheric lapse rate.

To compute the initial surface wind field we assume a balance between the surface pressure gradient, coriolis and frictional forces. Because the temperature lapse rate in the layer of topographic influence is initially the same as the free atmosphere lapse rate above, the expression for the surface pressure gradient force $\vec{P}$ reduces to (see Eq. 8)

$$\vec{P} = g \vec{\nabla}_\sigma Z_{850} - \frac{g(Z_{850} - Z_s)}{T_{850}} \vec{\nabla}_\sigma T_{850} \qquad 3.2$$

Note that this initial force is only dependent on height and

temperature variations at 850 mb.

Using the frictional parameterization described in Appendix I and the standard expression for the coriolis force, $\vec{C} = -f\vec{k} \times \vec{V}_s$, where f is the coriolis parameter and $\vec{k}$ is the unit normal vector at the suface, we can set up an expression for the balance between the pressure gradient, coriolis and frictional forces in which the only unknown is $\vec{V}_s$. Solving for $\vec{V}_s$ and using the T_s field calculated above, the model is ready for integration.

ASST. FOR ENV. SCIENCES
ASST. SEC. OF THE NAVY (R&D)
ROOM 5E731, THE PENTAGON
WASHINGTON, DC 20350

CHIEF OF NAVAL RESEARCH (2)
LIBRARY SERVICES, CODE 784
BALLSTON TOWER #1
800 QUINCY ST.
ARLINGTON, VA 22217

OFFICE OF NAVAL RESEARCH
CODE 422AT
ARLINGTON, VA 22217

OFFICE OF NAVAL RESEARCH
CODE 420
ARLINGTON, VA 22217

OFFICE OF NAVAL RESEARCH
CODE 422 CS
ARLINGTON, VA 22217

OFFICE OF NAVAL RESEARCH
CODE 422
ARLINGTON, VA 22217

OFFICE OF NAVAL RESEARCH
CODE 422 PO
ARLINGTON, VA 22217

OFFICE OF NAVAL RESEARCH
CODE 422 MM
ARLINGTON, VA 22217

OFFICE OF NAVAL TECHNOLOGY
MAT-0724, NAVY DEPT.
800 N. QUINCY ST.
ARLINGTON, VA 22217

CHIEF, ENV. SVCS. DIV.
OJCS (J-33)
RM. 2877K, THE PENTAGON
WASHINGTON, DC 20301

LIBRARY
NAVAL ARCTIC RESEARCH LAB
BARROW, AK 99723

COMMANDING OFFICER
NAVAL RESEARCH LAB
ATTN: LIBRARY, CODE 2620
WASHINGTON, DC 20390

COMMANDING OFFICER
OFFICE OF NAVAL RESEARCH
1030 E. GREEN ST.
PASADENA, CA 91101

OFFICE OF NAVAL RESEARCH
SCRIPPS INSTITUTION OF
OCEANOGRAPHY
LA JOLLA, CA 92037

COMMANDING OFFICER
FLENUMOCEANCEN
MONTEREY, CA 93943

DIRECTOR OF RESEARCH   (2)
U.S. NAVAL ACADEMY
ANNAPOLIS, MD 21402

NAVAL POSTGRADUATE SCHOOL
METEOROLOGY DEPT.
MONTEREY, CA 93943

LIBRARY
NAVAL POSTGRADUATE SCHOOL
MONTEREY, CA 93943

COMMANDER   (2)
NAVAIRSYSCOM
ATTN: LIBRARY (AIR-7226)
WASHINGTON, DC 20361

COMMANDER
NAVAIRSYSCOM (AIR-330)
WASHINGTON, DC 20361

COMMANDER
NAVAL WEAPONS CENTER
DR. A. SHLANTA, CODE 3918
CHINA LAKE, CA 93555

USAFETAC/TS
SCOTT AFB, IL 62225

AFGWC/DAPL
OFFUTT AFB, NE 68113

AFGL/LY
HANSCOM AFB, MA 01731

OFFICE OF STAFF METEOROLOGY
WESTERN SPACE & MISSILE
  CENTER (WE)
VANDENBERG AFB, CA 93437

COMMANDER & DIRECTOR
ATTN: DELAS-D
U.S. ARMY ATMOS. SCI. LAB
WHITE SAND MISSILE RANGE
WHITE SANDS, NM 88002

COMMANDING OFFICER
U.S. ARMY RESEARCH OFFICE
ATTN: GEOPHYSICS DIV.
P.O. BOX 12211
RESEARCH TRIANGLE PARK, NC
    27709

COMMANDER
COASTAL ENGINEERING RSCH CEN
KINGMAN BLDG.
FT. BELVOIR, VA 22060

ENGINEER TOPOGRAPHIC LABS
ATTN: ETL-GS-E
FT. BELVOIR, VA 22060

COMMANDER & DIRECTOR
ATTN: DELAS-AS
U.S. ARMY ATMOS. SCI. LAB
WHITE SANDS MISSILE RANGE,
NEW MEXICO 88002

COMMANDER & DIRECTOR
U.S. ARMY ATMOS. SCI. LAB.
ATTN: DELAS-AF
WSMR, NEW MEXICO 88002

DIRECTOR   (12)
DEFENSE TECH. INFORMATION
  CENTER, CAMERON STATION
ALEXANDRIA, VA 22314

DIRECTOR, ENV. & LIFE SCI.
OFFICE OF UNDERSECRETARY OF
  DEFENSE FOR RSCH & ENG E&LS
RM. 3D129, THE PENTAGON
WASHINGTON, DC 20505

DIRECTOR, TECH. INFORMATION
DEFENSE ADV. RSCH PROJECTS
1400 WILSON BLVD.
ARLINGTON, VA 22209

DR. JAMES E. OVERLAND
PACIFIC MARINE ENVIRONMENTAL
  LABORATORY/NOAA
7600 SANDPOINT WAY, NE
SEATTLE, WA 98115

FEDERAL COORD. FOR METEORO.
SERVS. & SUP. RSCH. (OFCM)
11426 ROCKVILLE PIKE
SUITE 300
ROCKVILLE, MD 20852

NATIONAL WEATHER SERVICE
WORLD WEATHER BLDG., RM 307
5200 AUTH ROAD
CAMP SPRINGS, MD 20023

DIRECTOR
GEOPHYS. FLUID DYNAMICS LAB
NOAA, PRINCETON UNIVERSITY
P.O. BOX 308
PRINCETON, NJ 08540

CHIEF
MESOSCALE APPLICATIONS BRANCH
NATIONAL EARTH SAT. SERV.
1225 W. DAYTON
MADISON, WI 53562

DIRECTOR
TECHNIQUES DEVELOPMENT LAB
GRAMAX BLDG.
8060 13TH ST.
SILVER SPRING, MD 20910

HEAD, ATMOS. SCIENCES DIV.
NATIONAL SCIENCE FOUNDATION
1800 G STREET, NW
WASHINGTON, DC 20550

LABORATORY FOR ATMOS. SCI.
NASA GODDARD SPACE FLIGHT CEN.
GREENBELT, MD 20771

EXECUTIVE SECRETARY, CAO
SUBCOMMITTEE ON ATMOS. SCI.
NATIONAL SCIENCE FOUNDATION
RM. 510, 1800 G. STREET, NW
WASHINGTON, DC 20550

DR. MARVIN DICKERSON
L-262, LLNL
P.O. BOX 808
LIVERMORE, CA 94550

DR. CLIFFORD F. MASS
DEPT. OF ATMOSPHERIC SCIENCES
UNIVERSITY OF WASHINGTON
SEATTLE, WA 98195

COLORADO STATE UNIVERSITY
ATMOSPHERIC SCIENCES DEPT.
ATTN: DR. WILLIAM GRAY
FORT COLLINS, CO 80523

CHAIRMAN
INSTITUTE OF ATMOS. PHYSICS
UNIV. OF ARIZONA
TUSCON, AZ 85721

SCRIPPS INSTITUTION OF
  OCEANOGRAPHY, LIBRARY
DOCUMENTS/REPORTS SECTION
LA JOLLA, CA 92037

ATMOSPHERIC SCIENCES DEPT.
UCLA
405 HILGARD AVE.
LOS ANGELES, CA 90024

CHAIRMAN, METEOROLOGY DEPT.
UNIVERSITY OF OKLAHOMA
NORMAN, OK 73069

CHAIRMAN, METEOROLOGY DEPT.
CALIFORNIA STATE UNIVERSITY
SAN JOSE, CA 95192

COLORADO STATE UNIVERSITY
ATMOSPHERIC SCIENCES DEPT.
ATTN: LIBRARIAN
FT. COLLINS, CO 80523

NATIONAL CENTER FOR ATMOS.
  RSCH., LIBRARY ACQUISITIONS
P.O. BOX 3000
BOULDER, CO 80302

UNIVERSITY OF WASHINGTON
ATMOSPHERIC SCIENCES DEPT.
SEATTLE, WA 98195

CHAIRMAN, METEOROLOGY DEPT.
PENNSYLVANIA STATE UNIV.
503 DEIKE BLDG.
UNIVERSITY PARK, PA 16802

FLORIDA STATE UNIVERSITY
ENVIRONMENTAL SCIENCES DEPT.
TALLAHASSEE, FL 32306

UNIVERSITY OF HAWAII
METEOROLOGY DEPT.
2525 CORREA ROAD
HONOLULU, HI 96822

DIRECTOR
COASTAL STUDIES INSTITUTE
LOUISIANA STATE UNIVERSITY
ATTN: O. HUH
BATON ROUGE, LA 70803

ATMOSPHERIC SCIENCES DEPT.
OREGON STATE UNIVERSITY
CORVALLIS, OR 97331

UNIVERSITY OF MARYLAND
METEOROLOGY DEPT.
COLLEGE PARK, MD 20742

CHAIRMAN
ATMOS. SCIENCES DEPT.
UNIVERSITY OF VIRGINIA
CHARLOTTESVILLE, VA 22903

CHAIRMAN
METEOROLOGY DEPT.
MASSACHUSETTS INSTITUTE OF
  TECHNOLOGY
CAMBRIDGE, MA 02139

CHAIRMAN, METEOROLOGY DEPT.
UNIVERSITY OF UTAH
SALT LAKE CITY, UT 84112

CHAIRMAN
METEOROLOGY & OCEANO. DEPT.
UNIVERSITY OF MICHIGAN
4072 E. ENGINEERING BLDG.
ANN ARBOR, MI 48104

TEXAS A&M UNIVERSITY
METEOROLOGY DEPT.
COLLEGE STATION, TX 77843

ATMOSPHERIC SCIENCES CENTER
DESERT RESEARCH INSTITUTE
P.O. BOX 60220
RENO, NV 89506

ATMOSPHERIC SCI. RSCH. CENTER
NEW YORK STATE UNIV.
1400 WASHINGTON AVE.
ALBANY, NY 12222

SYSTEMS & APPLIED SCI. CORP.
ATTN: LIBRARY, SUITE 500
6811 KENILWORTH AVE.
RIVERDALE, MD 20840

METEOROLOGY RESEARCH, INC.
464 W. WOODBURY RD.
ALTADENA, CA 91001

METEOROLOGY INTL., INC.
P.O. BOX 22920
CARMEL, CA 93922

ARVIN/CALSPAN ADVANCED TECH.
  CENTER
ATMOS. SCI./ENV. SCI. DEPT.
P.O. BOX 400
BUFFALO, NY 14225

83

THE RAND CORP LIBRARY
1700 MAIN ST.
SANTA MONICA, CA 90406

CONTROL DATA CORP.
METEOROLOGY DEPT. RSCH. DIV.
2800 E. OLD SHAKOPEE RD.
BOX 1249
MINNEAPOLIS, MN 55440

SCIENCE APPLICATIONS, INC.
205 MONTECITO AVE.
MONTEREY, CA 93940

OCEAN DATA SYSTEMS, INC.
2460 GARDEN ROAD
MONTEREY, CA 93940

THE EXECUTIVE DIRECTOR
AMERICAN METEORO. SOCIETY
45 BEACON ST.
BOSTON, MA 02108

AMERICAN METEORO. SOCIETY
METEOR. & GEOASTRO. ABSTRACTS
P.O. BOX 1736
WASHINGTON, DC 20013

MR. W. G. SCHRAMM/WWW
WORLD METEOROLOGICAL
  ORGANIZATION
CASE POSTALE #5, CH-1211
GENEVA, SWITZERLAND

LIBRARY, AUSTRALIAN NUMERICAL
METEOROLOGY RESEARCH CENTER
P.O. BOX 5089A
MELBOURNE, VICTORIA, 3001
AUSTRALIA

CHAIRMAN, METEOROLOGY DEPT.
MCGILL UNIVERSITY
805 SHERBROOKE ST., W.
MONTREAL, QUEBEC
CANADA H3A 2K6

LIBRARY/BIBLIOTHEQUE
ATMOSPHERIC ENVIRON. SERV.
4905 RUE DUFFERIN STREET
DOWNSVIEW, ONTARIO CANADA
M3H 5T4

INSTITUT FOR TEORETISK
  METEOROLOGI
HARALDSGADE 6
DK-2200 KOBEHAVN N
DENMARK

METEORO. OFFICE LIBRARY
LONDON ROAD
BRACKNELL, BERKSHIRE
RG 12 1SZ, ENGLAND

THE BRITISH LIBRARY
SCIENCE REFERENCE LIBRARY (A)
25 SOUTHAMPTON BLDGS.
CHANCERY LANE
LONDON WC2A 1AW

DEPARTMENT OF METEOROLOGY
UNIVERSITY OF READING
2 EARLYGATE, WHITEKNIGHTS
READING RG6 2AU
ENGLAND

EUROPEAN CENTRE FOR MEDIUM
RANGE WEATHER FORECASTS
SHINFIELD PARK, READING
BERKSHIRE RG29AX, ENGLAND

LIBRARY
FINNISH METEORO. INSTI.
BOX 503
SF-00101 HELSINKI 10
FINLAND

CENTRE DE RECHERCHE EN
  METEOROLOGIE
DYNAMIQUE (EERM/CRMD)
DIRECTION DE LA METEOROLOGIE
2 AVENUE RAPP
75007 PARIS, FRANCE

DIRECTOR
METEOROLOGISCHES INSTITUT
DER UNIVERSITAT BONN
53 BONN, AUF DEM HUGEL 20
FEDERAL REPUBLIC OF GERMANY

METEOROLOGISCHES INSTITUT
DER UNIVERSITAT KOELN
5000 KOELNWETERDIENST
FEDERAL REPUBLIC OF GERMANY

DIRECTOR, SWEDISH METEORO. &
  HYDROLOGICAL INSTITUTE
P.O. BOX 923
S-601, 19 NORRKOPING
SWEDEN

CHIEF ATMOS. SCIENCES DIV.
WORLD METEORO. ORGANIZATION
P.O. BOX 5
GENEVA 20, SWITZERLAND

U213870